Supplement of Geosci. Model Dev., 19, 5827–5855, 2026
https://doi.org/10.5194/gmd-19-5827-2026-supplement

Geoscientific Model Development
Open Access
EGU

Supplement of

Implementing belowground controls on nutrient uptake in ELMv2-SPRUCE improves representation of a boreal peatland ecosystem

Yaoping Wang et al.

Correspondence to: Yaoping Wang (wangy7@ornl.gov) and Jiafu Mao (maoj@ornl.gov)

S1 Supplementary Text

S1.1 Nutrient uptake modifications

S1.1.1 Preliminary notes

The same processes apply to nitrogen (N) and phosphorus (P). The description below (Sect. S1.1.2 to S1.1.10) focuses on N. The description for P can be obtained by substituting out all N by P in the text and equations, except when specifically pointed out. The capitalized letters in all the equations are modelled variables and will be explained as they appear. The meanings of subscripts are consistent throughout and are as follows:

i – soil layer

j – plant functional type (PFT), $j \in \{\text{spruce}, \text{tamarack}, \text{shrub}, \text{moss}\}$, or, when describing the new equations in ELM-MYCI, $j \in \{\text{spruce}, \text{tamarack}, \text{shrub}\}$, since moss is not modified

m – means the term is for soil decomposition

h - plant litter pool, $h \in \{lab, cel, lig\}$, lab – labile, cel – cellulose, lig – lignin

The model time step is Δt = 3600 seconds (1 hour). The lower-case letters that are not Δt or in the subscript are model parameters and will be explained as they appear. Parameter values are summarized in Table S2-Table S4 and main text Table 1.

S1.1.2 Nutrient uptake and plant C balance in ELM-OLD

Black + blue colours in Figure S1 show the calculations used to determine nutrient uptake in the default ELMv2-SPRUCE (ELM-OLD). Net photosynthesis is divided by the whole plant's C:N ratio to calculate the corresponding necessary N to support structural growth in leaf, stem, coarse root, and fine root C (Burrows et al., 2020). This growth demand for N is first met by retranslocation, and the remaining part becomes plant's demand for inorganic N, see Eq. (S1). Within a soil column, all the plant functional types (PFTs) and the soil decomposition processes compete for the same pool of soil inorganic N following the "Relative Demand" scheme (Burrows et al., 2020; Thornton and Rosenbloom, 2005). That is, the model first calculates a total potential N uptake by all the PFTs and soil decomposition (Eq. (S2)-(S3); also see Sect. S1.1.3). If the total potential N uptake is greater than the available soil inorganic N, the individual potential uptakes are all scaled down by the same column-level limitation factor, F_{Nlimit}, to obtain the actual uptakes, $N_{upt,act,j}$ (Eq. (S4)-(S6)). Under soil inorganic N or P limitation, plant structural growth is constrained to the lower of the two growth levels permitted by total N and P availability, i.e., the total of retranslocation and actual NP uptake, see Eq. (S7).

The calculation of each PFT's C balance is interwoven with the nutrient uptake calculations (Figure S2). At the centre is the nonstructural carbohydrates (NSC) pool, which receives new C from gross primary productivity (GPP), and supplies C to maintenance respiration (MR), excess respiration (XR), growth respiration (GR), structural C growth, and recovery of a virtual "XSMR" pool. MR reflects the metabolic energy spent to maintain a plant's regular functions, and increases approximately linearly with total living biomass. XR reflects the wasted energy due to nutrient limitation and increases exponentially up to a constant with the percentage of plant biomass existing as NSC. Both MR and XR also increase exponentially with temperature. GR reflects the energy spent to synthesize new biomaterials

for structural growth and is a small and constant fraction of structural growth. The "XSMR" pool is a virtual pool, defined for numerical purposes, to prevent the NSC pool from going negative when MR exceeds GPP for prolonged periods (e.g., in winter). Whenever MR > GPP, the unmet MR demand is subtracted from the XSMR pool instead of the NSC pool. This often causes the XSMR pool to go negative. To replenish the XSMR pool, when GPP > MR, some C is taken out of the NSC pool to slowly replenish it according to fixed rules. In this way, the XSMR pool has a small impact on net primary productivity (NPP), but it is not a physical pool or part of the plants' biomass.

$$N_{demand,inorg,j} = \max\left(\frac{C_{net}}{CN_j} - N_{retrans,j}, 0\right) \quad \forall j \tag{S1}$$

$$N_{upt,pot,j} = N_{demand,inorg,j} \quad \forall j \tag{S2}$$

$$N_{upt,pot} = N_{upt,pot,m} + \sum_j N_{upt,pot,j} \tag{S3}$$

$$F_{Nlimit} = \min\left(N_{soil}/(N_{upt,pot} \cdot \Delta t), 1\right) \tag{S4}$$

$$N_{upt,act,j} = F_{Nlimit} N_{upt,pot,j} \quad \forall j \tag{S5}$$

$$N_{upt,act,m} = F_{Nlimit} N_{upt,pot,m} \tag{S6}$$

$$\Delta C_{structural,j} = \begin{cases} C_{net} \cdot \Delta t & \text{if } \min(F_{Nlimit}, F_{Plimit}) = 1 \\ \min\left(\dfrac{CN_j \cdot \Delta t}{N_{upt,act,j} + N_{retrans,j}}, \dfrac{CP_j \cdot \Delta t}{P_{upt,act,j} + P_{retrans,j}}\right) & \text{if } \min(F_{Nlimit}, F_{Plimit}) < 1 \end{cases} \tag{S7}$$

$C_{net,j}$ – incoming net photosynthesis, g C m^{-2} s^{-1}

CN_j – the whole plant's C:N ratio, unitless

$N_{retrans,j}$ – N supply from retranslocation, g N m^{-2} s^{-1}

$N_{demand,inorg,j}$ – plant demand for inorganic N, g N m^{-2} s^{-1}

$N_{upt,pot,j}$ – potential plant inorganic N uptake, g N m^{-2} s^{-1}

$N_{upt,pot,m}$ – potential soil decomposition inorganic N uptake, g N m^{-2} s^{-1}

$N_{upt,pot}$ – total potential plant and soil decomposition inorganic N uptake, g N m^{-2} s^{-1}

N_{soil} – size of the column-level inorganic N pool (the sum of NH_4^+, NO_3^-, and biological N fixation; for P, this is soluble P [PO_4^{3-}]), g N m^{-2}

F_{Nlimit} – column-level N-limitation factor, unitless

$N_{upt,act,j}$ – actual plant inorganic N uptake, g N m^{-2} s^{-1}

$N_{upt,act,m}$ – actual soil decomposition inorganic N uptake, g N m^{-2} s^{-1}

$\Delta C_{structural,j}$ – structural growth of the plant in the time step, g C m^{-2}

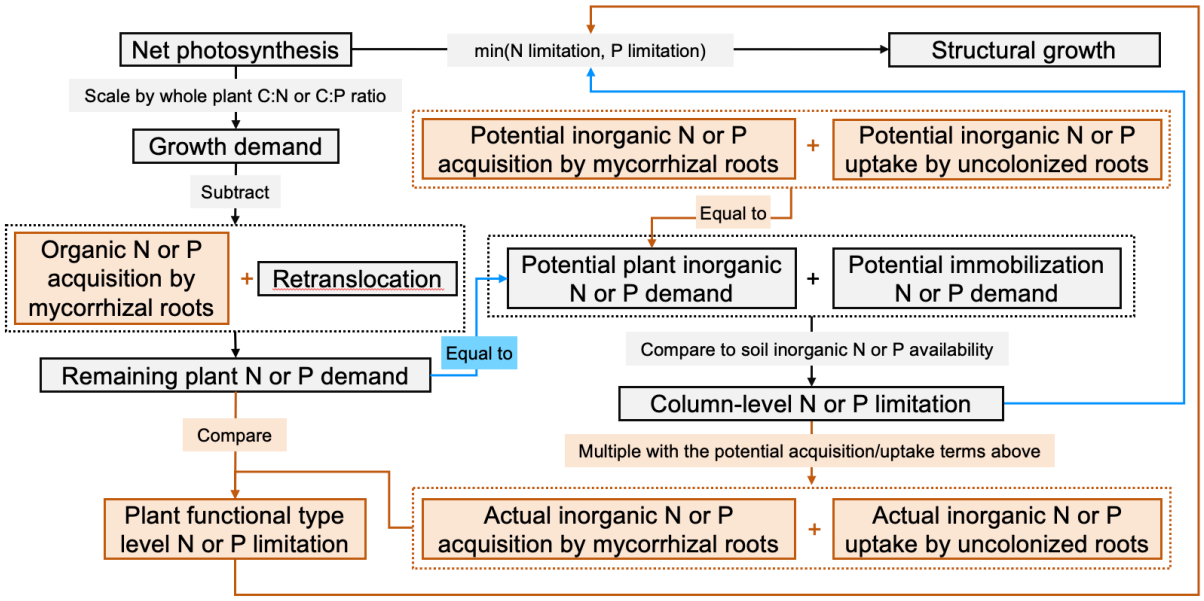

Figure S1. Nutrient uptake processes by the vascular plant functional types in ELM-OLD and ELM-MYCI. Boxes with edge are modelled quantities, lines and boxes without edge are calculations. Black boxes and lines are shared processes, blue ones exist only in ELM-OLD, and orange ones exist only in ELM-MYCI.

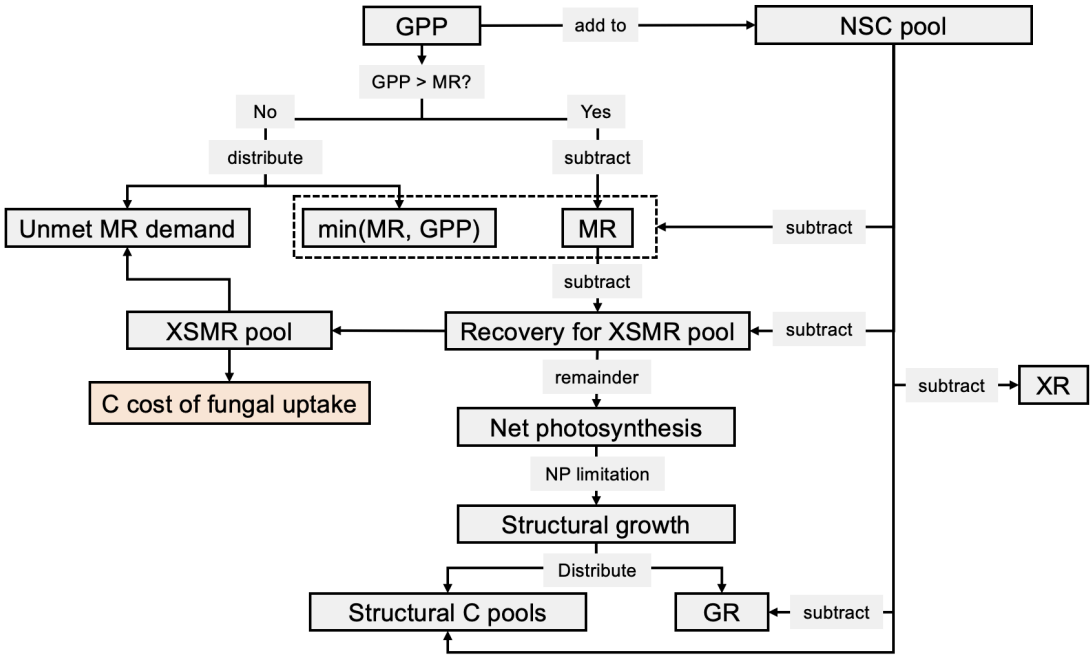

Figure S2. Relationship between the terms involved in the N and P uptake calculations (net photosynthesis and structural growth) and the terms involved in C-balance calculations (the other terms in this figure). Black boxes are terms shared by ELM-OLD and ELM-MYCI. The orange box is a new flux out of the XSMR pool in ELM-MYCI. Abbreviations: GPP – gross primary productivity, MR – maintenance respiration, XR – excess respiration, GR – growth respiration, NSC – nonstructural carbohydrates.

S1.1.3 Nutrient limitation of the soil-decomposition process in ELM-OLD and ELM-MYCI

Although soil decomposition processes are not modified in this study, and the full scheme is described elsewhere (Burrows et al., 2020; Oleson et al., 2013), a brief overview is provided here to contextualize heterotrophic respiration (HR) and its dependence on nutrient availability. ELMv2-SPRUCE uses the Converging Trophic Cascade scheme, which has one coarse woody debris pool, three plant litter pools (conceptualized as labile, cellulose, and lignin), and four soil organic matter (SOM) pools (Burrows et al., 2020; Oleson et al., 2013). C flows from upstream to downstream pools, in the approximate order of woody debris → plant litter → faster-turnover SOM → slower-turnover SOM, following first-order exponential decay. The C:N and C:P ratios of the coarse woody debris and plant litter pools are flexible and determined by the input plant materials. The C:N and C:P ratios of the SOM pools are fixed parameters (Table S2).

During each transformation, a fraction of the upstream carbon is released as CO_2, in proportion to the pool size and the transformation rate. HR is calculated as the sum of these CO_2 fluxes across all transformations and soil layers. Each transformation also generates N and P demands ($N_{upt,pot,m}$ in Eq. (S3), immobilization demand in Figure S1), because the upstream pools generally have higher C:N and C:P ratios than the downstream pools. To satisfy these stoichiometric requirements, additional N and P must be obtained from the soil inorganic pool. Nutrient limitation of the transformation rate, and thus HR, occurs when the available soil inorganic N or P is insufficient to meet the combined demands of plants and decomposition (Eq. (S4)).

S1.1.4 Overview of the nutrient uptake and plant C balance in ELM-MYCI

In the modified ELMv2-SPRUCE (ELM-MYCI), we split the nutrient uptake processes of the vascular PFTs (spruce, tamarack, and shrubs) into three pathways: (1) direct inorganic nutrient uptake by uncolonized fine roots ($PATH^{root}$), (2) indirect inorganic nutrient acquisition by mycorrhizal roots ($PATH^{myc,inorg}$), and (3) indirect nutrient acquisition from organic sources by mycorrhizal roots ($PATH^{myc,org}$). This split is based on the idea that EcM fungal mantle can prevent fine roots from accessing the soil solution (He et al., 2018). The uncolonized fine roots can only use $PATH^{root}$, whereas the fungi-colonized fine roots can only use $PATH^{myc,inorg}$ and $PATH^{myc,org}$. Pathways (2) and (3) are mycorrhizal-implicit. They do not consider fungal biomass dynamics or explicit exchanges of C-N-P between the plant host and fungi. Instead, they treat the fungal uptake of inorganic nutrient, or mining of organic nutrient, and subsequent transfer to the plant host via the colonized fine roots as a lumped process. The plant host pays a C cost for the fungi-mediated nutrient acquisitions from the XSMR pool (Figure S2 orange box), but this cost is not allocated to fungal biomass or soil respiration because doing so appropriately would require modifying the soil decomposition scheme (Sect. S1.1.3). Nutrient uptake and the C balance for the non-vascular *Sphagnum* moss remains the same as in ELM-OLD. The competition between all PFTs and soil decomposition also remains the same as in ELM-OLD, Eq. (S3)-(S7).

We embed the three pathways into the broader model as shown in Figure S1 (orange boxes). We first modify Eq. (S1) to let the growth demand for N be first met by retranslocation and $PATH^{myc,org}$, Eq. (S8). The remainder becomes the plant's demand for inorganic N. This order of subtraction gives the plant a preference of organic N over inorganic N, which we deem acceptable for the boreal peatland ecosystem because it has abundant organic matter. Under the

current code structure of ELMv2-SPRUCE, removing this assumption will require revising both the nutrient competition and soil decomposition calculations, which is beyond the scope of this study. We then replace Eq. (S2) with Eq. (S9), where the new potential inorganic N uptake is the sum of two potential uptake terms, one via $PATH^{root}$ and one via $PATH^{myc,inorg}$. After scaling down the potential inorganic N uptake by soil N availability, Eq. (S4)-(S6), we obtain the actual inorganic N uptake via $PATH^{root}$ and $PATH^{myc,inorg}$. The sum of retranslocation, the actual inorganic N uptake via fine roots, the actual inorganic N acquisition via mycorrhizal roots, and the organic N acquisition via mycorrhizal roots becomes the total N supplied to the plants for structural growth, Eq. (S10). With those modifications, we obtain PFT-specific nutrient-limitation factors, Eq. (S11), as opposed to only the column level one in Eq. (S4) in ELM-OLD.

$$N_{demand,inorg,j} = \max\left(\frac{C_{net}}{CN_j} - N_{retrans,j} - N_{myc,org,j}, 0\right) \quad \forall j \tag{S8}$$

$$N_{upt,pot,j} = N_{froot,j} + N_{myc,inorg,j} \tag{S9}$$

$$\Delta C_{structural,j} = \begin{cases} C_{net} \cdot \Delta t & \text{if } F_{Nlimit} = 1 \\ \dfrac{CN_j \cdot \Delta t}{N_{upt,act,j} + N_{retrans,j} + N_{myc,org,j}} & \text{if } F_{Nlimit} < 1 \end{cases} \tag{S10}$$

$$F_{Nlimit,j} = \begin{cases} 1 & \text{if } N_{demand,inorg,j} = 0 \\ \dfrac{N_{upt,act,j}}{N_{demand,inorg,j}} & \text{if } N_{demand,inorg,j} > 0 \end{cases} \tag{S11}$$

$N_{myc,org,j}$ – N acquisition from organic sources through mycorrhizal roots, g N m^{-2} s^{-1}

$N_{myc,inorg,j}$ – potential inorganic N acquisition through mycorrhizal roots, g N m^{-2} s^{-1}

$N_{froot,j}$ – potential uptake of inorganic N through uncolonized fine roots, g N m^{-2} s^{-1}

$F_{Nlimit,j}$ – PFT-specific N limitation factor, unitless

S1.1.5 Colonization rates by ectomycorrhizal and ericoid fungi

Operationalizing Eq. (S8)-(S11) requires modelling the fraction of roots that are uncolonized, i.e. using $PATH^{root}$, and colonized, i.e. using $PATH^{myc,inorg}$ and $PATH^{myc,org}$. At the SPRUCE site, observations found that the total abundance of dark fungal hyphae, which could be ErM in origin and from *Cenococcum geophilum*, declined by 75-100% from the unheated to the warmest chamber (Defrenne et al., 2021). SPRUCE observations also found shrub roots to vastly increase in total and specific root length in the warmer enclosures, indicating a shift towards the do-it-yourself strategy (Malhotra et al., 2020; Weber et al., 2025). Other past experiments found peatland ericaceous shrubs to uptake less N via ErM fungi under inorganic N addition (Vesala et al., 2021). Based on these studies, we have relatively high confidence that ErM colonization of shrub roots decreases towards the warmer enclosures. Observed root-tip colonization rates for the EcM trees are very noisy and do not show clear trends across warming treatments (Figure S10). Also, past experiments found both increases and decreases in EcM colonization under N additions, possibly related to the amount of added N and water conditions (Table S1).

Based on the above information, we initially tested two ways to model fungal colonization rates: a linear function of annual average water table depth, or a linear function of annual average soil inorganic N content. The first approach turned out to be inviable because it induced little gradient across the treatment chambers. Therefore, we chose the

second approach, see Eq. (S12). We use the average soil inorganic N content over 0-30 cm because it is the rooting zone at the SPRUCE site (Iversen et al., 2018). For parameter optimization, we constrain the slope of response to be $b_j < 0$ for ErM colonization of shrubs but does not impose such constraint for the trees (main text Table 1). We choose not to include a soil P content control on mycorrhizal colonization in this study, because the study site's dependence on P is less well-understood and fewer prior studies have focused on P (Table S1) (Bashian-Victoroff et al., 2025), but we put a zero-coefficient into the code as placeholder for potential addition of P control in the future.

$$M_{myc,j} = \max\left(0, \min\left(1, a_j + b_j N_{soil,annavg}\right)\right) \quad \text{(S12)}$$

$M_{myc,j}$ – fraction of fine roots colonized by mycorrhizal fungi, unitless

$N_{soil,annavg}$ – annual average soil inorganic N ($NH_4^+ + NO_3^-$) content in the rooting zone, g N m^{-3}

a_j – intercept parameter

b_j – slope parameter

Table S1. Review of previous studies on the influences of moisture and nutrients to EcM colonization of boreal trees.

Plant type	Treatment	Outcome	Study
Pinus sylvestris	N addition, 3-50 kg N ha^{-1} yr^{-1}	No change in colonization	(Forsmark et al., 2021)
Forest stands including sugar maple, beech, yellow birch, black spruce, moss and ErM shrub understory	N addition, 9-85 kg N ha^{-1} yr^{-1}	Small increase in abundance, possibly driven by tree growth	(Renaudin et al., 2023)
Picea mariana	N addition, 9-30 kg N ha^{-1} yr^{-1}	Small increase in fraction of colonized root tips	(Rossi et al., 2012)
Picea asperata	Watering gradient (40-100% field capacity) x N addition gradient (0-400 kg N ha^{-1} yr^{-1})	Higher EcM colonization rates in drier treatments. Lower colonization rates under N addition	(Xie et al., 2021)
Pinus sylvestris	N addition at 100 kg N ha^{-1} yr^{-1}	Lower EcM colonization rates	(Högberg et al., 2010)

S1.1.6 Common environmental multipliers

We apply the following common environmental multipliers when modelling the uptake/acquisition of all three pathways: soil temperature, soil moisture, and the plant's N limitation in the previous time step. The former two multipliers are soil layer specific. The soil temperature multiplier is a conventional Q_{10} function, Eq. (S13). The soil moisture multiplier, from (Frolking et al., 2002), is selected because the formula lets both dry soil and excess moisture to inhibit nutrient uptake, Eq. (S14). The inhibition of waterlogging on nutrient uptake is supported by observational evidence (Struyf et al., 2011). The third multiplier is a feedback mechanism that makes the modelled PFTs ramp up

uptake/acquisition rates in a nutrient-poor environment while preventing them from infinitely accumulating nutrients when demands are already met, Eq. (S15). It is weakly supported by experimental observations that high tissue nutrient concentrations inhibit plant nutrient uptake (Glass et al., 2002). Figure S3 shows the form of Eq. (S15) under various α-values. In the absence of suitable observational references and noting that the parameter does not have a large impact on model results in one-at-a-time sensitivity analysis (Figure S6), we chose $\alpha = 1.5$.

$$\mathcal{F}\left(T_{soi,i}\right) = q_{10}^{(T_{soi,i}-10)/10} \tag{S13}$$

$$\mathcal{F}\left(\Theta_{soi,i}\right) = \begin{cases} 1 - \left(\dfrac{\theta_{opt} - \Theta_{soi,i}}{\theta_{opt}}\right)^2 & \text{if } \Theta_{soi,i} \leq \theta_{opt} \\ 1 - 0.5\left(\dfrac{\Theta_{soi,i} - \theta_{opt}}{1 - \theta_{opt}}\right) & \text{if } \Theta_{soi,i} > \theta_{opt} \end{cases} \tag{S14}$$

$$\mathcal{F}\left(F_{Nlimit,j}\right) = \frac{\alpha}{F_{Nlimit,j}^2 + \alpha - 1} \tag{S15}$$

$T_{soi,i}$ – soil temperature of layer i, °C

q_{10} – Q_{10} parameter for temperature sensitivity of nutrient uptake

$\Theta_{soi,i}$ – volumetric soil water content in soil layer i, $m^3\ m^{-3}$

θ_{opt} – optimal soil volumetric water content for nutrient uptake, $m^3\ m^{-3}$

α – parameter controlling the feedback of excessive nutrient uptake on uptake rates

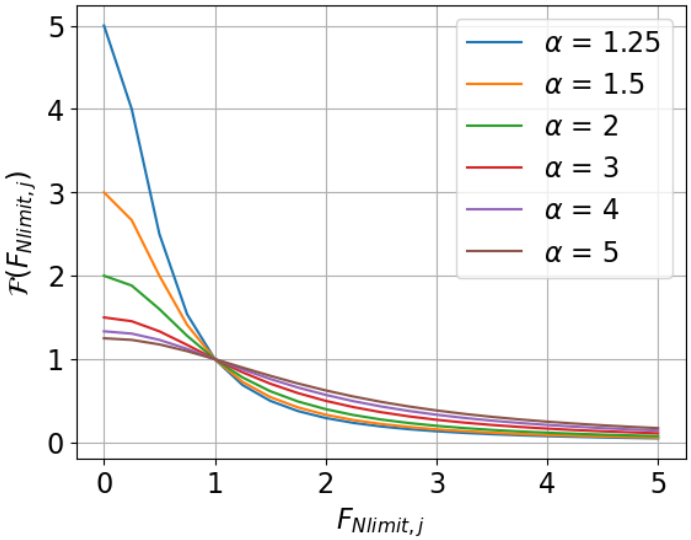

Figure S3. Visualization of the N limitation multiplier, Eq. (S15), at different parameter values.

S1.1.7 Acquisition of nutrient from soil inorganic and organic sources via mycorrhizal roots

Mycorrhizal fungi growth, and hence their ability to obtain soil nutrients, depend partially on C transfer from the plants (He et al., 2018, 2021; Shao et al., 2023). In our implicit approach, we account for this phenomenon by applying a multiplier based on NSC availability (Eq. (S16)) and an upper bound based on the availability of new photosynthates (Sect. S1.1.8) on the acquisition rates of $PATH^{myc,inorg}$ and $PATH^{myc,org}$. In Eq. (S16), when a PFT has high NSC

compared to its structural biomass C in leaf and fine root, the multiplier approaches one, and in the opposite situation, zero.

$$\mathcal{F}(C_{ns,j}) = \frac{k_{nsc} C_{ns,j}}{k_{nsc} C_{ns,j} + C_{froot,j} + C_{leaf,j}} \quad \text{(S16)}$$

k_{nsc} – unitless sensitivity parameter

$C_{ns,j}$ – nonstructural carbohydrates content, g C m^{-2}

$C_{froot,j}$ – displayed fine-root carbon biomass, g C m^{-2}

$C_{leaf,j}$ – displayed leaf-carbon biomass, g C m^{-2}

In each soil layer, the potential N acquisition rate via PATH^{myc,org} is a function of the amount of ErM- or EcM-colonized fine-root biomass, $M_{myc,j} C_{froot,j} f_{froot,i,j}$, the environmental multipliers (Sect. S1.1.6), and the NSC multiplier, see Eq. (S17). The fraction of fine-root biomass in each soil layer, $f_{froot,i,j}$, is set using linear vertical rooting profiles, Eq. (S18), that are fitted on in situ minirhizotron data (Weber et al., 2025). The actual N acquisition rate via PATH^{myc,org} in each soil layer is limited by the sizes of soil organic N pools and the fraction of those pools that can be accessed, Eq. (S19)-(S20), using the high bound 0.0001 in the CoupModel (He et al., 2018). The total actual N acquisition rate via PATH^{myc,org} is calculated as the sum over all soil layers, Eq. (S21), followed by a final adjustment that prevents unnecessary uptake during nighttime and dormancy (see Sect. S1.1.8).

We restrict the mycorrhizal-available soil organic N pools to the three plant litter pools in the soil decomposition scheme (Sect. S1.1.3). This is because those three pools allow flexible C:N and C:P ratios, while the four SOM pools require fixed C:N and C:P ratios. To allow N and P acquisition from the SOM pools require considering how much C to release as fungal respiration. However, the current first-order decomposition processes in ELMv2-SPRUCE have no explicit microbial pools; as such, it is uncertain how much of the HR already reflects fungal respiration in the real world. There may also be difference between EcM and ErM in the fraction of released C (Clemmensen et al., 2021). Due to those difficulties, we leave the treatment of the SOM pools to future model development.

In the real world, ErM has limited ability to degrade lignin/lignin-like *Sphagnum* phenolics and other complex biopolymers (Ward et al., 2022). However, the lignin pool in ELMv2-SPRUCE is more of an abstract pool based on a decay rate than the real lignin compound (Oleson et al., 2013). Preventing the ErM-shrub association from accessing this pool will make its accessibility to organic N and P unrealistically low. Therefore, we allow the EcM-tree and ErM-shrub association to access all the litter pools.

$$N_{myc,pot,org,i,j} = u_{N,myc,j} M_{myc,j} C_{froot,j} F_{froot,i,j} \mathcal{F}(T_{soi,i}) \mathcal{F}(\Theta_{soi,i}) \mathcal{F}(F_{Nlimit,j}) F(C_{ns,j}) \quad \text{(S17)}$$

$$F_{froot,i,j} = \begin{cases} a_{root}(z_i - z_{i-1}) & \text{if } i > 1 \text{ or } b_{root} < 0 \\ a_{root} z_i + b_{root} & \text{if } i = 1 \text{ and } b_{root} > 0 \end{cases} \quad \text{(S18)}$$

$$N_{avail,org,i,j} = \frac{0.0001}{\Delta t}\left(O_{N,i,lab} + O_{N,i,cel} + O_{N,i,lig}\right) \quad \text{(S19)}$$

$$N_{pre,myc,org,i,j} = \min\left(N_{myc,pot,org,i,j}, N_{avail,org,i,j}\right) \quad \text{(S20)}$$

$$N_{pre,myc,org,j} = \sum_{i=1}^{10} N_{pre,myc,org,i,j} \quad \text{(S21)}$$

$N_{myc,pot,org,i,j}$ – potential N acquisition from organic sources via mycorrhizal roots in one soil layer, g N m^{-2}

$u_{N,myc,j}$ – the maximum organic N acquisition rate per unit colonized fine-root biomass, gN g C^{-1} s^{-1}

$F_{froot,i,j}$ – fraction of fine root in one soil layer, unitless

a_{root} – slope parameter of cumulative fine-root distribution

b_{root} – intercept parameter of cumulative fine-root distribution

z_i – the bottom depth of the soil layer, m

$N_{avail,org,i,j}$ – soil organic N pool size available to the plant-fungi association, g N m^{-2}

$O_{N,i,lab}$ – soil organic N pool size in the labile litter pool in the soil layer, g N m^{-2}

$O_{N,i,cel}$ – soil organic N pool size in the cellulose litter pool in the soil layer, g N m^{-2}

$O_{N,i,lig}$ – soil organic N pool size in the lignin litter pool in the soil layer, g N m^{-2}

$N_{pre,myc,org,i,j}$ – the pre-adjustment actual acquired N from organic sources via mycorrhizal roots in one soil layer, g N m^{-2}

$N_{pre,myc,org,j}$ – the pre-adjustment actual acquired N from organic sources via mycorrhizal roots over all the soil layers, gN m^{-2}

Because inorganic N is much more scarce than organic N in peatland ecosystems, we limit the potential N acquisition rate by $PATH^{myc,inorg}$ by a Michaelis-Menten multiplier, Eq. (S22). The other terms in the calculation, Eq. (S23), are the same as those in the calculation of potential organic N acquisition rate, Eq. (S17). The potential acquisition rates are summed up over all the soil layers, Eq. (S24), and subject to a final adjustment (see Sect. S1.1.8).

Constraining the rate constant ($v_{N,fungi,j}$) and half-saturation point ($k_{N,j}$) in the Michaelis-Menten multiplier is difficult. Experimentally observed rate constants vary by three orders of magnitude (10^{-12} to 10^{-9} g N cm^{-2} s^{-1} and 10^{-13} to 10^{-10} g P cm^{-2} s^{-1}), and half-saturation points vary by one order of magnitude (0.25-3.338 g N m^{-3} water, 0.049-0.17 g P m^{-3} water) (Table S5-Table S6). Therefore, we first use hand-tuning to determine approximate guesses for those parameters. Then, during parameter optimization, we set the upper and lower bounds to be [0.1, 10] of the initial guesses of the rate constants, and [0.5, 2] of the initial guesses of the half-saturation points (Table S4, main text Table 1).

We do not distinguish between NH_4^+ and NO_3^- when calculating the N acquisition rate by $PATH^{myc,inorg}$. The concentration of NO_3^- is near-zero compared to NH_4^+ in the SPRUCE ecosystem (main text Figure 2), and plants exhibit plasticity and acclimation in their N-form preference (Chalk and Smith, 2021; Daryanto et al., 2019). As such, we deem differentiating between these two chemical forms to be an unnecessary complexity.

$$\mathcal{F}_j\left(N_{conc,i}\right) = \frac{N_{conc,i}}{k_{N,j} + N_{conc,i}} \tag{S22}$$

$$N_{myc,pot,inorg,i,j} = v_{N,myc,j} M_{myc,j} C_{froot,j} F_{froot,i,j} \mathcal{F}_j\left(N_{conc,i}\right) \mathcal{F}\left(T_{soi,i}\right) \mathcal{F}\left(\Theta_{soi,i}\right) \mathcal{F}\left(F_{Nlimit,j}\right) F\left(C_{ns,j}\right) \tag{S23}$$

$$N_{pre,myc,inorg,j} = \sum_{i=1}^{10} N_{myc,pot,inorg,i,j} \tag{S24}$$

$N_{conc,j}$ – soil inorganic N concentration ($NH_4^+ + NO_3^-$; for P, PO_4^{3-}) in one soil layer, g N m^{-3}

$k_{N,j}$ – half-saturation point for inorganic N uptake/acquisition, including via mycorrhizal roots and uncolonized fine roots, g N m^{-3}

$N_{myc,pot,inorg,i,j}$ – potential inorganic N acquisition via mycorrhizal roots in one soil layer, g N m^{-2} s^{-1}

$v_{N,myc,j}$ – maximum inorganic N acquisition rate per unit colonized fine-root biomass, g N g C^{-1} s^{-1}

$N_{pre,myc,inorg,j}$ – pre-adjustment inorganic N acquisition via mycorrhizal roots over all the soil layers, g N m^{-2} s^{-1}

S1.1.8 Upper bound on the nonstructural carbohydrate cost of N acquisition via mycorrhizal roots

In addition to letting the plant's NSC abundance influence the acquisition rates of PATH^{myc,inorg} and PATH^{myc,org}, Eq. (S16), we impose an upper bound on the total N acquisition from inorganic and organic sources via mycorrhizal associations due to their C cost to the plants. That is, the total acquired N from organic and inorganic sources, multiplied by a constant factor, c_N, must not exceed 50% of the net photosynthesis at each time step (C_{net}, defined in the beginning of Sect. S1.1.2), see Eq. (S25)-(S29). We choose the 50% threshold following the maximum value found in a previous meta-analysis (Hawkins et al., 2023). The use of net photosynthesis in the upper bound prevents nutrient acquisition during the night and during winter dormancy. The scaled-down inorganic N acquisition, combined with direct fine-root N uptake, undergo competition with soil decomposition, which is already described in Eq. (S9) and (S5). The total C cost to the plant is equal to the greater value between the total C cost of N acquisitions and the total C cost of P acquisitions via PATH^{myc,inorg} and PATH^{myc,org}, Eq. (S30).

We subtract the C cost from the virtual XSMR pool (see Sect. S1.1.2) in this study, which has a damped negative effect on the NSC pool – if all other model terms are held constant, a more negative XSMR pool will incur more frequent replenishments from the NSC pool to the XSMR pool (Figure S2). We do not subtract from the NSC pool directly, because negative NSC pool sizes will cause numerical problems in ELMv2-SPRUCE, and because it is desirable to keep the model insensitive to c_N and c_P at this stage. The C cost of fungal nutrient uptake is not commonly reported in the literature and probably varies with environmental conditions. For example, (Hobbie and Högberg, 2012) found c_N ranges from 0-180 g C g N^{-1} based on isotopic theoretical calculations. They further suggest that as the environment becomes more N-abundant, the fungi allow a greater fraction of their assimilated N to be transferred to the plant, resulting in a decline in the C cost.

$$C_{pre,N,myc,j} = c_N\left(N_{pre,myc,org,i,j} + N_{pre,myc,inorg,j}\right) \quad \text{(S25)}$$

$$N_{myc,org,j} = N_{pre,myc,org,j} \min\left(\frac{C_{pre,N,myc,j}}{0.5C_{net,j}}, 1\right) \quad \text{(S26)}$$

$$N_{myc,org,i,j} = N_{pre,myc,org,i,j} \min\left(\frac{C_{pre,N,myc,j}}{0.5C_{net,j}}, 1\right) \quad \forall i \quad \text{(S27)}$$

$$N_{myc,inorg,j} = N_{pre,myc,inorg,j} \min\left(\frac{C_{pre,N,myc,j}}{0.5C_{net,j}}, 1\right) \quad \text{(S28)}$$

$$N_{myc,inorg,i,j} = N_{pre,myc,inorg,i,j} \min\left(\frac{C_{pre,N,myc,j}}{0.5C_{net,j}}, 1\right) \quad \forall j \quad \text{(S29)}$$

$$C_{myc,j} = \max\left(c_N\left(N_{myc,org,j} + F_{Nlimit}N_{myc,inorg,j}\right), c_P\left(P_{myc,org,j} + F_{Plimit}P_{myc,inorg,j}\right)\right) \quad \text{(S30)}$$

$C_{pre,N,myc,j}$ – pre-adjustment C cost of N acquisition from inorganic and organic sources via mycorrhizal roots to a PFT, g C m^{-2} s^{-1}

c_N – C cost per unit acquired N via mycorrhizal foots, g C g N^{-1}, $c_N = 20$; for P, $c_P = 200$

$N_{myc,org,j}$ – adjusted total rate of N acquisition from organic sources over all the soil layers via mycorrhizal roots, g N m^{-2} s^{-1}

$N_{myc,org,i,j}$ – adjusted rate of N acquisition from organic sources in one soil layer via mycorrhizal roots, g N m^{-2} s^{-1}

$N_{myc,inorg,j}$ – adjusted total rate of inorganic N acquisition over all the soil layers via mycorrhizal roots, g N m^{-2} s^{-1}

$N_{myc,inorg,i,j}$ – adjusted rate of inorganic N acquisition from one soil layer via mycorrhizal roots, g N m^{-2} s^{-1}

$C_{myc,j}$ – C cost of nutrient acquisition via mycorrhizal roots to a PFT, g C m^{-2} s^{-1}

S1.1.9 Reduction of soil organic N content due to the acquisition of mycorrhizal roots

To model the reduction in soil organic N content due to the acquisition by mycorrhizal roots, we distribute the final adjusted organic N acquisition, Eq. (S26), summed over all the vascular PFTs, across the three accessed litter pools proportional to pool size, see Eq. (S31). The organic C in those pools are not changed.

$$\Delta O_{N,i,h} = \begin{cases} -N_{myc,org,i,j}\dfrac{O_{N,i,h}}{O_{N,i,lab} + O_{N,i,cel} + O_{N,i,lig}}\Delta t & \forall h \in \{lab, cel, lig\} \\ & \text{if } j \in \{\text{spruce, tamarack}\} \\ -N_{myc,org,i,j}\dfrac{O_{N,i,h}}{O_{N,i,lab} + O_{N,i,cel}}\Delta t & \forall h \in \{lab, cel\} \\ & \text{if } j = \text{shrub} \end{cases} \quad \text{(S31)}$$

$\Delta O_{N,i,h}$ – change in the size of the plant litter pool in one soil layer in one time step, g N m^{-2}

S1.1.10 Direct uptake of inorganic nutrients by uncolonized fine roots

In modelling direct fine-root uptake of inorganic nutrients, we included a root surface area term, Eq. (S32), from the PEATBOG model (Wu and Blodau, 2013). The term is related to measurable root economic traits, here radius and density (Bergmann et al., 2020), enabling distinction between the thinner shrub roots and the coarser tree roots at the SPRUCE site (Iversen et al., 2018). We parameterize the fine-root radius and density directly using the observed values at the SPRUCE site for first- and second-order fine roots, which are primarily responsible for the adsorptive function (Iversen et al., 2017; McCormack et al., 2015). The other multipliers in the uptake rate formula parallel those of inorganic N acquisition via mycorrhizal roots, except for the absence of the NSC multiplier, see Eq. (S33) and Eq. (S23). We use the same half-saturation point, $k_{N,j}$, for $PATH^{root}$ and $PATH^{myc,inorg}$ (Eq. (S22)), in order to limit model complexity in the presence of high observational uncertainty (Table S6). The uptake rates are modelled for each soil layer and summed up, Eq. (S34).

$$A_{froot,i,j} = \frac{0.01 C_{froot,j} F_{froot,i,j}}{r_j^2 \rho_j} \quad \text{(S32)}$$

	$N_{froot,i,j} = v_{N,froot,j}(1 - M_{myc,j})A_{froot,i,j}\mathcal{F}_j(N_{conc,i})\mathcal{F}(T_{soi,i})\mathcal{F}(\Theta_{soi,i})\mathcal{F}(F_{Nlimit,j})$	(S33)
	$N_{froot,j} = \sum_{i=1}^{10} N_{froot,i,j}$	(S34)

$A_{froot,i,j}$ – total surface area of fine roots in one soil layer, $cm^2\ m^{-2}$

r_j – fine-root radius of the PFT, cm

ρ_j – fine-root density of the PFT, g C cm^{-3}

$v_{N,froot,j}$ – maximum fine-root inorganic N uptake rate per unit uncolonized root surface area, g N $cm^{-2}\ s^{-1}$

S1.2 Removal of pretreatment variability

For each variable among $AGNPP_{spruce}$, $AGNPP_{tamarack}$, annual maximum LAI of spruce, and annual maximum LAI of tamarack, we fit an ordinary least-squares regression:

	$X^{post} \sim I(CO_2) + T_{air} + Year + X^{pre} + I(CO_2) \times T_{air} + I(CO_2) \times Year$	(S35)

, where X^{post} is the post-treatment value in a year and enclosure, $I(CO_2)$ indicates whether that enclosure is treated with elevated CO_2 ($I(CO_2)$=1) or not ($I(CO_2)$=0), T_{air} is the annual mean air temperature in the year and enclosure, X^{pre} is the observed year 2014 pre-treatment value in the enclosure. After fitting this initial formula, we drop all the insignificant terms using $p \leq 0.05$ criteria and re-fit a final regression. If the pretreatment term is still significant in the final regression, we remove its effect as $X^{adj} = X^{post} - b(X^{pre} - \bar{X}^{pre})$, where b is the regression coefficient of X^{pre}, $\bar{X}^{pre}$ is the average pre-treatment value across all enclosure, and X^{adj} is the adjusted observed value.

S1.3 Upscaling of the NEE of the shrub-moss community

Automated chamber measurements of soil-air CO_2 exchanges were performed using two chambers per enclosure at the SPRUCE site during 2022 and 2023. The chambers are 50 cm in diameter and 25 cm high aboveground (15 cm inserted beneath soil) (Stelling et al., 2024). The 2022 data span only a couple of months in each enclosure, while the 2023 data span most of April to October. Therefore, we only upscaled the 2023 data to obtain a more reliable set of growing-season (2023-05-01 to 2023-10-31) average $NEE_{shrubmoss}$.

We gapfilled the chamber-level observed fluxes by using a Q_{10} function to model the ecosystem respiration component and a rectangular hyperbolic function for the GPP component, following the conventional approach for NEE gapfilling (Lasslop et al., 2010). Previous work on the moss community at SPRUCE further found that water table depth (W_h) is an important covariate to include in those functions (Walker et al., 2017). Therefore, we tested multiple formulas and selected the best fit using the Akaike Information Criteria (AIC). For ecosystem respiration, we compared Q_{10}-only [Eq. (S36)] and Q_{10}+W_h [Eq. (S37)] formulas (Walker et al., 2017). For GPP, we compared PAR-only [Eq. (S38)] and PAR+W_h [Eq. (S39)] formulas (Walker et al., 2017), as well as a PAR+W_h+Tair [Eq. (S40)] formula that models the temperature effect on GPP as a unimodal function, $\mathcal{F}(T_{air})$. The temperature effect function is from the well-accepted Vegetation Photosynthesis Model (Glauch et al., 2025).

	$R_{eco} = r_{base} \cdot \left(Q_{10,eco}\right)^{\frac{T_{soil}-15}{10}}$	(S36)
	$R_{eco} = (r_{base} + r_w W_h) \cdot \left(Q_{10,eco}\right)^{\frac{T_{soil}-15}{10}}$	(S37)
	$GPP = \frac{\alpha \cdot PAR \cdot g_{max}}{\alpha \cdot PAR + g_{max}}$	(S38)
	$GPP = \frac{\alpha \cdot PAR \cdot (g_{max} + g_w W_h)}{\alpha \cdot PAR + (g_{max} + g_w W_h)}$	(S39)
	$GPP = \frac{\alpha \cdot PAR \cdot (g_{max} + g_w W_h)}{\alpha \cdot PAR + (g_{max} + g_w W_h)} \mathcal{F}(T_{air})$	(S40)
	$\mathcal{F}(T_{air}) = \begin{cases} 0 & \text{if } T_{air} > t_{max} \text{ or } T_{air} < t_{min} \\ \frac{(T_{air} - t_{min}) \cdot (T_{air} - t_{max})}{(T_{air} - t_{min}) \cdot (T_{air} - t_{max}) - \left(T - t_{opt}\right)^2} & \text{if } t_{max} < T_{air} < t_{min} \end{cases}$	(S41)

R_{eco} – ecosystem respiration, μmol CO_2 m^{-2} s^{-1}

r_{base} – base rate of ecosystem respiration, μmol CO_2 m^{-2} s^{-1}

$Q_{10,eco}$ – the Q10 parameter to be estimated

T_{soil} – soil temperature at 5 cm depth, °C

r_{wt} – the sensitivity of base rate of ecosystem respiration to water table depth, μmol CO_2 m^{-2} s^{-1} cm^{-1}

W_h – water table depth relative to the hollow surface, cm

GPP – gross primary productivity, μmol CO_2 m^{-2} s^{-1}

α – light use efficiency, μmol CO_2 μmol^{-1} photons

PAR – photosynthetically active radiation, μmol photons m^{-2} s^{-1}

g_{max} – maximum GPP at light saturation, μmol CO_2 m^{-2} s^{-1}

T_{air} – air temperature at 0.5 m height, matching the height of the collar measurements, °C

t_{min}, t_{max}, t_{opt} – maximum, minimum, and optimal temperature parameters for temperature response of GPP

The fitting was performed using nonlinear least squares (Levenberg-Marquardt algorithm via scipy.optimize.curve_fit in Python) separately for each plot. The two small chambers in each plot were pooled. The sign convention is NEE = R_{eco} – GPP. The PAR covariate was measured inside the collars (Stelling et al., 2024). The other environmental covariates (5 cm soil temperature, 0.5 m air temperature, and water table depth) are from the SPRUCE environmental data (Hanson et al., 2016). We aggregated the flux measurements from 15-minute to 30-minute intervals because the water table depth covariate was only observed at 30-minute intervals. We used 0.5 m air temperature for the GPP fit because it is the lowest height at which air temperature was observed at SPRUCE and closest to the aboveground collar height (25 cm). The R_{eco} fitting used nighttime CO_2 flux, defined as when PAR < 50 μmol m^{-2} s^{-1} and flux > 0. The Q_{10}+W_h formula clearly outperformed the Q_{10}-only formula, with lower root mean squared error, lower AIC, and better seasonality (Figure S4). Therefore, we used the fitted Q_{10}+W_h to gapfill a continuous R_{eco} series spanning night- and day-time. We then subtracted the daytime R_{eco} from the observed flux to obtain daytime GPP. The PAR-only formula on this GPP was clearly the worst, while the PAR+W_h and PAR+W_h+T_{air} formulas had similar performances, but PAR+W_h+T_{air} had slightly lower root mean squared errors and AIC in all except two chambers with low GPP

(+0.00 ambient CO_2 and +2.25 elevated CO_2) (Figure S5). Therefore, we gapfilled the GPP values using the PAR+W_h+T_{air}. The observed $NEE_{shrubmoss}$ was then calculated from these gapfilled R_{eco} and GPP and averaged between 2023-05-01 and 2023-10-31.

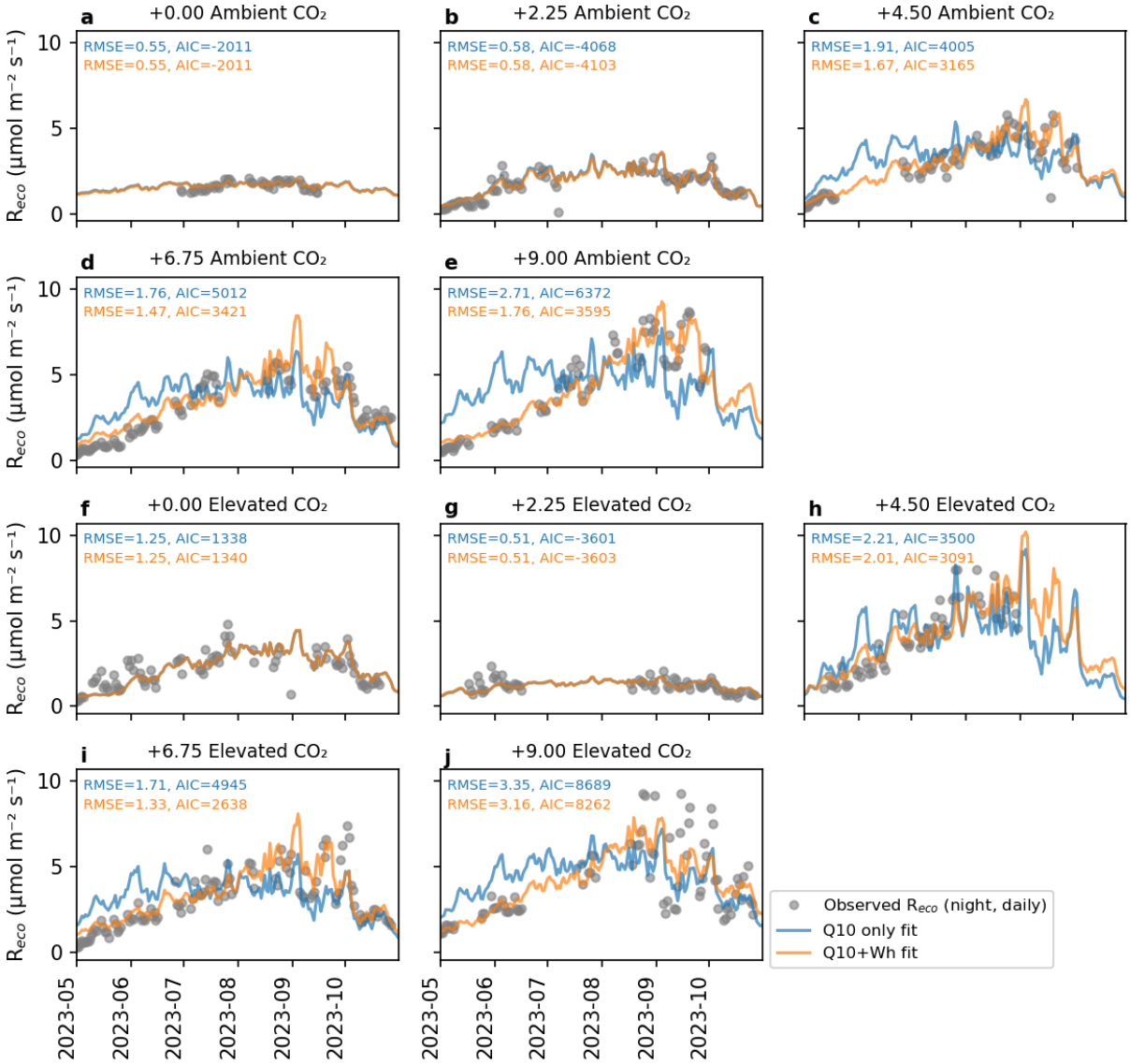

Figure S4. Goodness-of-fit of the Q_{10}-only [Eq. (S36)] and Q_{10}+W_h [Eq. (S37)] formulas on ecosystem respiration (R_{eco}). RMSE – root mean squared error. AIC – Akaike Information Criteria. Each plot was fitted individually.

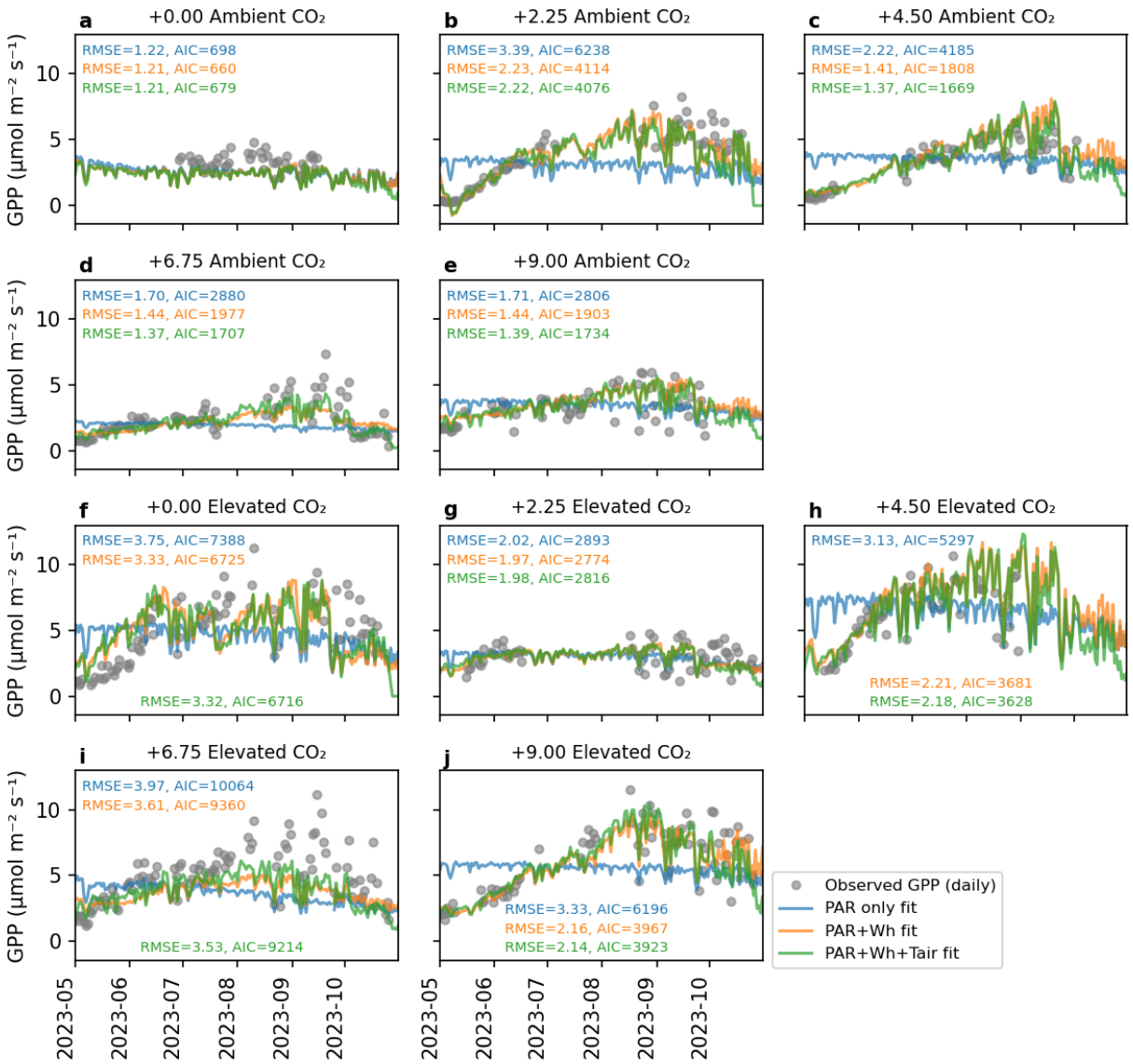

Figure S5. Goodness-of-fit of the PAR-only [Eq. (S38)], PAR+W_h [Eq. (S39)], and PAR+W_h+Tair [Eq. (S40)] formulas on gross primary productivity (GPP). RMSE – root mean squared error. AIC – Akaike Information Criteria. Each plot was fitted individually.

S2 Supplementary Tables

Table S2. Biogeochemistry-related parameters in ELM-OLD that are updated in this study using observed or manually tuned values.

Parameter name (Unit)	Explanation	Plant functional type	Values	Source
leaf_long (year)	leaf longevity for evergreen leaves	Spruce	5	(Salmon et al., 2021)
froot_cn (gC gN^{-1})	Fine root C:N ratio	Spruce	35	(Iversen et al., 2021)
		Tamarack	40	
		Shrub	55	
livewd_cn (gC gN^{-1})	Live wood C:N ratio	Spruce	90	(Phillips et al., 2017)
		Tamarack	60	
		Shrub	85	
leaf_cp (gC gP^{-1})	Leaf C:P ratio	Spruce	655.78	
		Tamarack	655.78	
		Shrub	594.72	
cn_s1 (gC gN^{-1})	C:N ratio of the first SOM pool	-	22	(Griffiths et al., 2017)
cn_s2 (gC gN^{-1})	C:N ratio of the second SOM matter pool	-	22	(Griffiths et al., 2017)
cn_s3 (gC gN^{-1})	C:N ratio of the third SOM matter pool	-	20	(Griffiths et al., 2017)
cn_s4 (gC gN^{-1})	C:N ratio of the fourth SOM pool	-	20	(Griffiths et al., 2017)
r_mort ($year^{-1}$)	Whole-plant turnover rate	Spruce	0.2	Manually tuned to match observed biomass magnitude
		Tamarack	0.2	
		Shrub	0.12	

Table S3. Biogeochemistry-related preexisting parameters in ELM-OLD that are optimized. The upper and lower bounds are determined based on previous ranges (Griffiths et al., 2017; Meng et al., 2021; Ricciuto et al., 2018).

Parameter name in ELMv2-SPRUCE (Unit)	Explanation	Plant functional type	Range	Optimized values in ELM-OLD_{optim}
mbbopt (1)	Ball-Berry slope of conductance-photosynthesis relationship, unstressed	Spruce	[4.5, 13.5]	10.26
		Tamarack		9.96
		Shrub		11.33
vcmaxhd (J mol^{-1})	Deactivation energy for Vcmax	Spruce	[191000, 210000]	197844
		Tamarack		206246

		Shrub		197588
flnr (1)	Fraction of leaf N in in Rubisco enzyme	Spruce	[0.05, 0.30]	0.08376
		Tamarack		0.19381
		Shrub		0.29826
slatop (m^2 gC^{-1})	Specific leaf area at top of canopy	Spruce	[0.0051, 0.0095]	0.00909
		Tamarack	[0.01708, 0.02604]	0.02572
		Shrub	[0.01666, 0.0308]	0.01985
br_mr_pft (gC gN^{-1} s^{-1})	Base rate of maintenance respiration	Spruce	[10^{-6}, 5*10^{-6}]	3.283*10^{-6}
		Tamarack		1.319*10^{-6}
		Shrub		4.234*10^{-6}
q10_mr_pft (1)	Q_{10} of maintenance respiration	Spruce	[1.2, 3.8]	2.322
		Tamarack		3.209
		Shrub		1.369
froot_leaf (gC gC^{-1})	Ratio of fine root to leaf allocation	Spruce	[0.3, 1.3]	1.015
		Tamarack		1.085
		Shrub		0.628
stem_leaf (n/a)	Parameter controlling stem-to-leaf allocation ratio	Spruce	[-0.5, -0.1]	-0.4796
		Tamarack		-0.3084
decomp_depth_efolding (m)	e-folding depth for reduction in decomposition	-	[0.3, 1.0]	0.3039
q10_hr (1)	Q_{10} for heterotrophic respiration	-	[1.4, 2.5]	1.922
mino2lim (1)	Minimum anaerobic decomposition rate as a fraction of potential aerobic rate	-	[0.0001, 0.05]	0.003131

Table S4. Newly added parameters in ELM-MYCI that are manually tuned.

Symbol (Unit)	**Equation appeared in**	**Plant functional type**	**Value**	**Range in one-at-a-time sensitivity analysis**	**Source**
a_j (1)	Eq. (S12)	Spruce	0.7	[0.2, 0.8]	Manually tuned based on observed ranges (Rossi et al., 2012; Xie et al., 2021)
		Tamarack	0.5		

θ_{opt} (1)	Eq. (S14)	-	0.6	[0.3, 0.9]	(Frolking et al., 2002)
α (1)	Eq. (S15)	-	1.5	[0.75, 2.25]	Selected based on comparing a range of values in Figure S3
k_{nsc} (1)	Eq. (S16)	-	2	[1, 3]	Manually tuned
a_{root} (1)	Eq. (S18)	Spruce	11.7605	-	Fitted to observed fine root depth distribution at SPRUCE (Weber et al., 2025)
		Tamarack	11.7605	-	
		Shrub	7.5535	-	
b_{root} (1)	Eq. (S18)	Spruce	-0.11713	-	
		Tamarack	-0.11713	-	
		Shrub	0.04493	-	
$u_{N,fungi,j}$ (gN gC^{-1} s^{-1})	Eq. (S17)	Tamarack	1.0209*10^{-8}	[1.0209*10^{-9}, 1.0209*10^{-7}]	Manually tuned to ensure all PFTs grow
		Shrub	3.5748 *10^{-8}	[3.5748*10^{-9}, 3.5748*10^{-7}]	
$k_{N,j}$ (gN m^{-3})	Eq. (S22)	Spruce	7	[3.5, 14]	Manually tuned to approximately match annual average simulated soil inorganic N levels
		Tamarack	7		
		Shrub	7		
$k_{P,j}$ (gP m^{-3})	Phosphorus counterpart of Eq. (S22)	Tamarack	0.004955	[0.002478, 0.009911]	Manually tuned to approximately match annual average simulated soil inorganic P levels
		Shrub	0.004955		
$v_{N,fungi,j}$ (gN gC^{-1} s^{-1})	Eq. (S23)	Spruce	4.5977*10^{-9}	[4.5977*10^{-10}, 4.5977*10^{-8}]	Manually tuned with reference to values in (He et al., 2021; Shao et al., 2023)
		Shrub	3.3289*10^{-9}	[3.3289*10^{-10}, 3.3289*10^{-8}]	
$v_{P,fungi,j}$ (gP gC^{-1} s^{-1})	Phosphorus counterpart of Eq. (S23)	Tamarack	2.7566*10^{-10}	[2.7567*10^{-11}, 2.7567*10^{-9}]	
		Shrub	8.0369*10^{-10}	[8.0369*10^{-11}, 8.0369*10^{-9}]	
c_P (gC gP^{-1})	Phosphorus counterpart of Eq. (S25), Eq. (S30)	-	200	[100, 1000]	Manually tuned in line with the typical order-of-magnitude N:P ratio (~10:1) in soil-plant systems

r_j (cm)	Eq. (S32)	Spruce	0.012	-	Unpublished observed data (Iversen et al., 2018)
		Tamarack	0.018	-	
		Shrub	0.0045	-	
ρ_j (gC cm^{-3})	Eq. (S32)	Spruce	0.16	-	Unpublished observed data, assuming 46% C in biomass (Iversen et al., 2018)
		Tamarack	0.15 gC cm^{-3}	-	
		Shrub	0.09 gC cm^{-3}	-	
$v_{N,froot,j}$ (gN gC^{-1} s^{-1})	Eq. (S33)	Spruce	4.2538*10^{-12}	[4.2538*10^{-13}, 4.2538*10^{-11}]	Manually tuned with reference to values in (Shao et al., 2023; Wu and Blodau, 2013)

Table S5. Review of experimentally measured uptake rates by fungi-colonized and uncolonized fine roots. If the paper reported a maximum rate constant, that value is used here; otherwise, the fastest measured rate is used. The converted values in gN or gP cm^{-2} s^{-1} use Eq. (S32) to make the original values reported in different units comparable. The conversion used 0.015 cm radius and 0.155 gC cm^{-3} density for trees, and 0.0045 cm radius and 0.09 gC cm^{-3} density for shrub and herbs based on the SPRUCE-observed values in Table S4.

Plant species	**Nutrient species**	**Value in original unit**	**Converted value (gN or gP cm^{-2} s^{-1})**	**Converted value (gN or gP gC^{-1} s^{-1})**	**Source**
Picea asperata, uncolonized roots	NH_4^+	130 pmol cm^{-2} s^{-1}	1.820*10^{-9}	2.401*10^{-7}	(Xie et al., 2021)
	NO_3^-	90 pmol cm^{-2} s^{-1}	1.260*10^{-9}	1.662*10^{-7}	
Picea asperata, EcM colonized roots	NH_4^+	30 pmol cm^{-2} s^{-1}	4.200*10^{-10}	5.540*10^{-8}	
	NO_3^-	20 pmol cm^{-2} s^{-1}	2.800*10^{-10}	3.693*10^{-8}	
Douglas fir, uncolonized roots	NH_4^+	22 nmol m^{-2} s^{-1}	3.080*10^{-11}	4.063*10^{-9}	(Hawkins et al., 2008)
	NO_3^-	25 nmol m^{-2} s^{-1}	3.500*10^{-11}	4.616*10^{-9}	
Lodgepole pine, uncolonized roots	NH_4^+	14 nmol m^{-2} s^{-1}	1.960*10^{-11}	2.585*10^{-9}	
	NO_3^-	20 nmol m^{-2} s^{-1}	2.800*10^{-11}	3.693*10^{-9}	
Hardwood trees	NH_4^+	8 μmol g root^{-1} hr^{-1}	2.359*10^{-10}	3.111*10^{-8}	(Sanders-DeMott et al., 2018)
Hardwood trees	NO_3^-	0.25 μ mol g root^{-1} hr^{-1}	7.371*10^{-12}	9.722*10^{-10}	
Eriophorum vaginatum	NH_4^+	13.7 μmol g^{-1} hr^{-1}	2.111*10^{-11}	5.328*10^{-8}	(Chapin et al., 1993)

Vaccinium macrocarpon, uncolonized roots	NO_3^-	0.017 μ mol g^{-1} DW min^{-1}	$1.572*10^{-12}$	$3.967*10^{-9}$	(Kosola et al., 2007)
Vaccinium macrocarpon, ErM colonized roots	NO_3^-	0.16 μ mol g^{-1} DW min^{-1}	$1.479*10^{-11}$	$3.733*10^{-8}$	
Pinus sylvestris, uncolonized	PO_4^{3-}	0.2 nmol s^{-1} g^{-1} d. wt root	$4.701*10^{-11}$	$6.200*10^{-9}$	(Colpaert et al., 1999)
Pinus sylvestris, colonized whole plant	PO_4^{3-}	1 nmol s^{-1} g^{-1} d. wt root	$2.350*10^{-10}$	$3.100*10^{-8}$	
Pinus sylvestris, uncolonized	PO_4^{3-}	0.08 nmol g^{-1} s^{-1}	$1.880*10^{-11}$	$2.480*10^{-9}$	(Van Tichelen and Colpaert, 2000)
Pinus sylvestris, colonized whole plant	PO_4^{3-}	0.13-0.62 nmol g^{-1} s^{-1}	$3.055*10^{-11}$ - $1.457*10^{-10}$	$4.030*10^{-9}$ - $1.922*10^{-8}$	
Calluna vulgaris, colonized by endophytes and ErM	PO_4^{3-}	1500 pg mg root FW^{-1} $hour^{-1}$	$1.360*10^{-13}$	$3.432*10^{-10}$	(Arndal et al., 2013)

Table S6. Review of experimentally measured half-saturation point in uptake kinetics.

Value in original unit	**Converted value (gN m^{-3} water)**	**Plant species**	**Nutrient species**	**Source**
242 μmol kg^{-1}	3.338	*Eriophorum vaginatum*	NH_4^+	(Chapin et al., 1993)
Only linear relationship observed	-	*Vaccinium macrocarpon*, uncolonized roots	NH_4^+	(Kosola et al., 2007)
Only linear relationship observed	-	*Vaccinium macrocarpon*, uncolonized roots	NO_3^-	
34.54 μmol kg^{-1}	0.48	*Vaccinium macrocarpon*, colonized roots	NH_4^+	
17.75 μmol kg^{-1}	0.25	*Vaccinium macrocarpon*, ErM colonized roots	NO_3^-	

12.1 μmol kg^{-1}	0.17	*Pinus sylvestris*, uncolonized	PO_4^{3-}	(Van Tichelen and Colpaert, 2000)
3.5-10.2 μmol kg^{-1}	0.049-0.143	*Pinus sylvestris*, colonized whole plant	PO_4^{3-}	

Table S7. Sphagnum cover (%) by year and treatment chamber (Norby et al., 2019; Weston D. 2020, 2021 unpublished data).

Treatment	2016	2017	2018	2019	2020	2021
+0.00	25	24.5	24.9	23.7	24.6	24.6
+2.25	25	21.1	21.1	24	19	19
+4.50	25	19.4	19.3	12.3	9.2	9.2
+6.75	25	21.3	10.1	8.1	4	4
+9.00	24	8.9	3.8	3.6	0.6	0.6
+0.00 CO_2	25	25	24	23.3	23.3	23.3
+2.25 CO_2	24.3	17.4	16.5	14.5	14.5	14.5
+4.50 CO_2	25	4.8	5.7	3.7	1.2	1.2
+6.75 CO_2	22	12.1	14	10.1	7.1	7.1
+9.00 CO_2	23.1	11.2	4.2	3.7	1.7	1.7
Ambient	25	25	25	25	25	25

Table S8. Measured *Sphagnum* or shrub aboveground biomass in the automated chambers divided by the measured *Sphagnum* or shrub aboveground biomass in the corresponding SPRUCE plot.

Treatment	*Sphagnum* ratio	Shrub ratio
+0.00	0.64	0.16
+2.25	0.81	0.05
+4.50	0.43	0.16
+6.75	0.37	0.32
+9.00	0.48	1.49
+0.00 CO_2	1.04	0.18
+2.25 CO_2	1.01	0.31
+4.50 CO_2	0.58	2.36
+6.75 CO_2	0.59	1.54
+9.00 CO_2	0.96	0.78

S3 Supplementary Figures

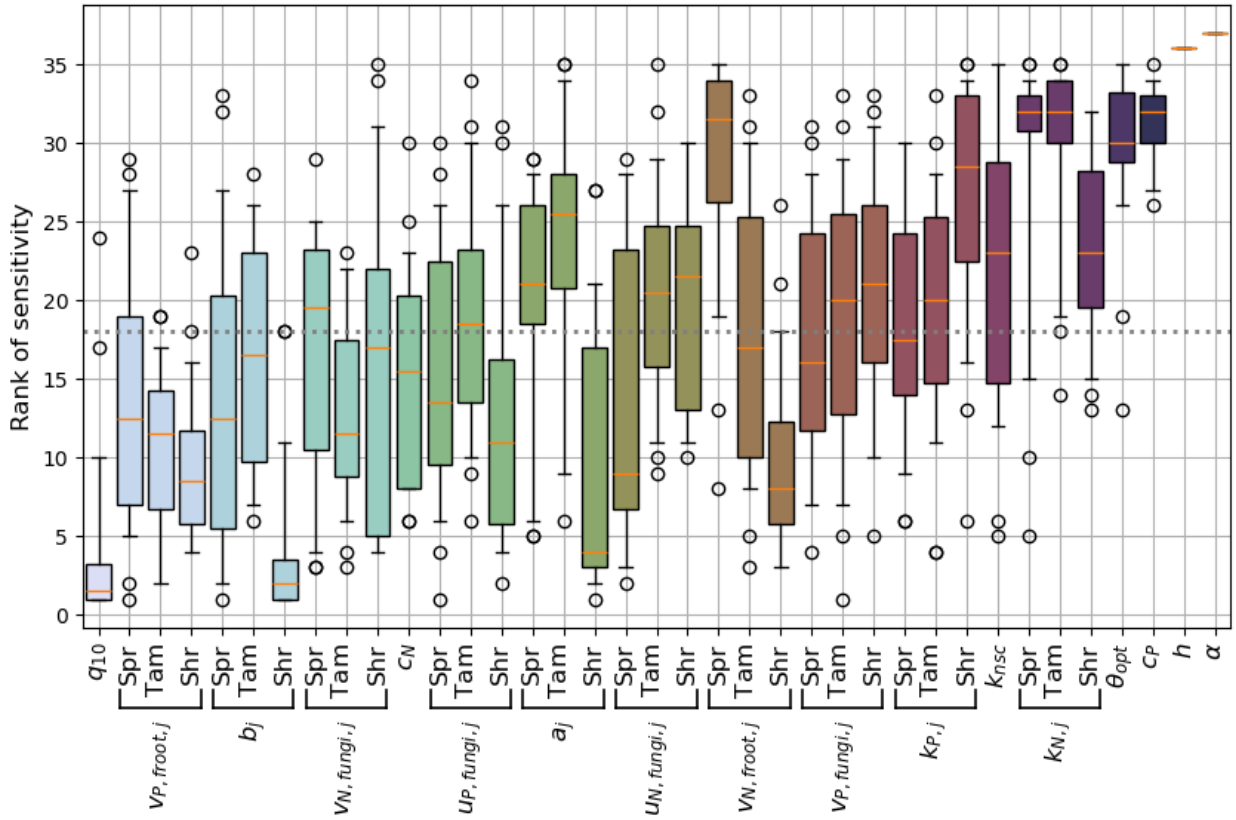

Figure S6. Rank of the sensitivity of carbon fluxes to the newly added parameters in ELM-MYCI. A smaller rank means greater sensitivity. Parameters that have PFT-specific values are grouped together and labelled by Spr – spruce, Tam – tamarack, Shr – shrub. Boxplots show the [min, 5th percentile, 25th percentile, median, 75th percentile, 95th percentile, max] of the ranks across the means and slopes of all the independent carbon flux variables in ambient and elevated CO_2 enclosures. Parameters/PFT-specific values ranked below the threshold line (horizontal, dashed grey) are selected for ensemble simulation and optimization.

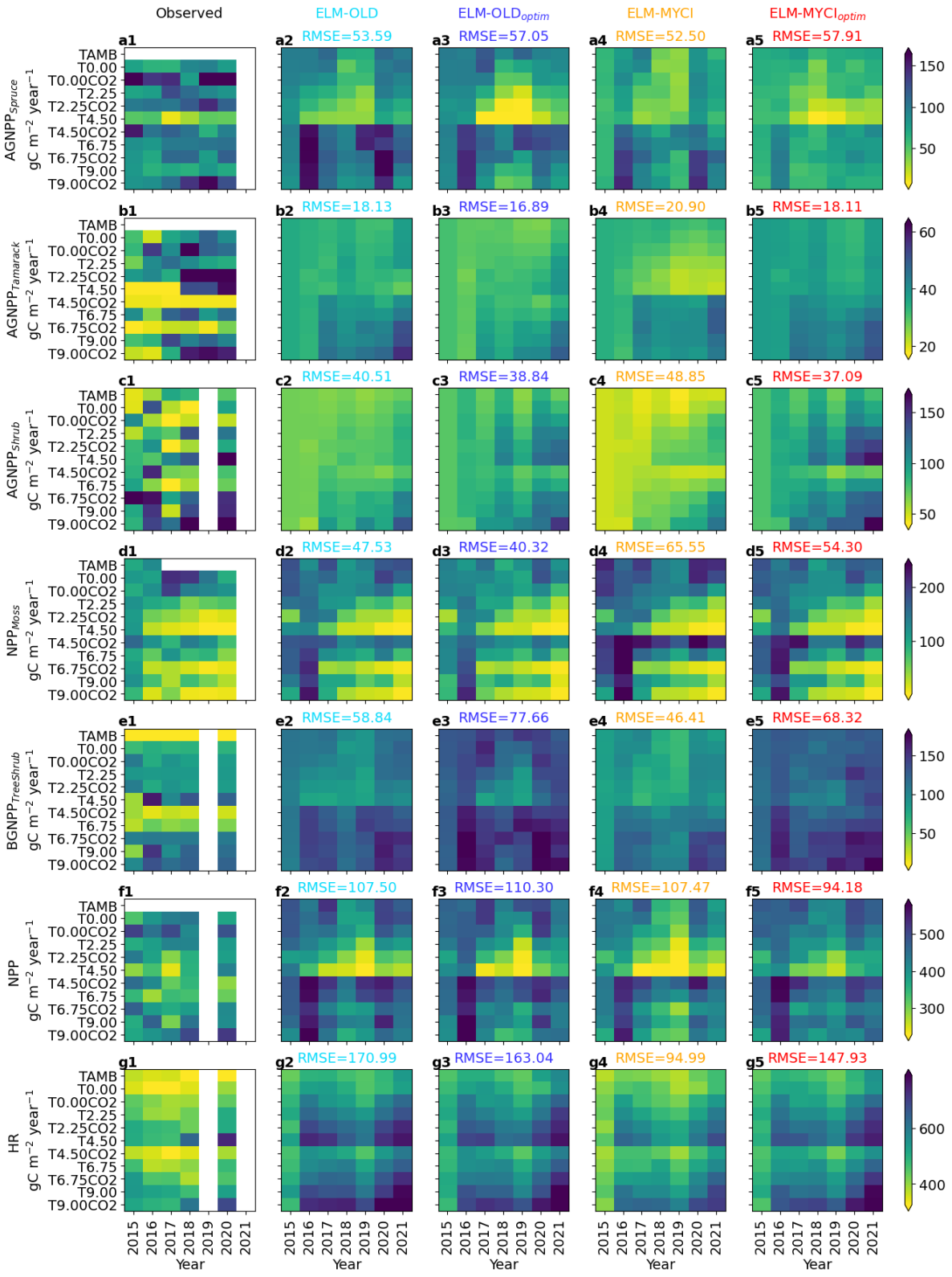

Figure S7. Observed annual time series of selected C fluxes during the calibration period, and the corresponding simulated levels. The root mean squared error (RMSE) values were calculated between each model setup and the observation, on all the data points displayed in one panel (i.e. across all the years and treatments).

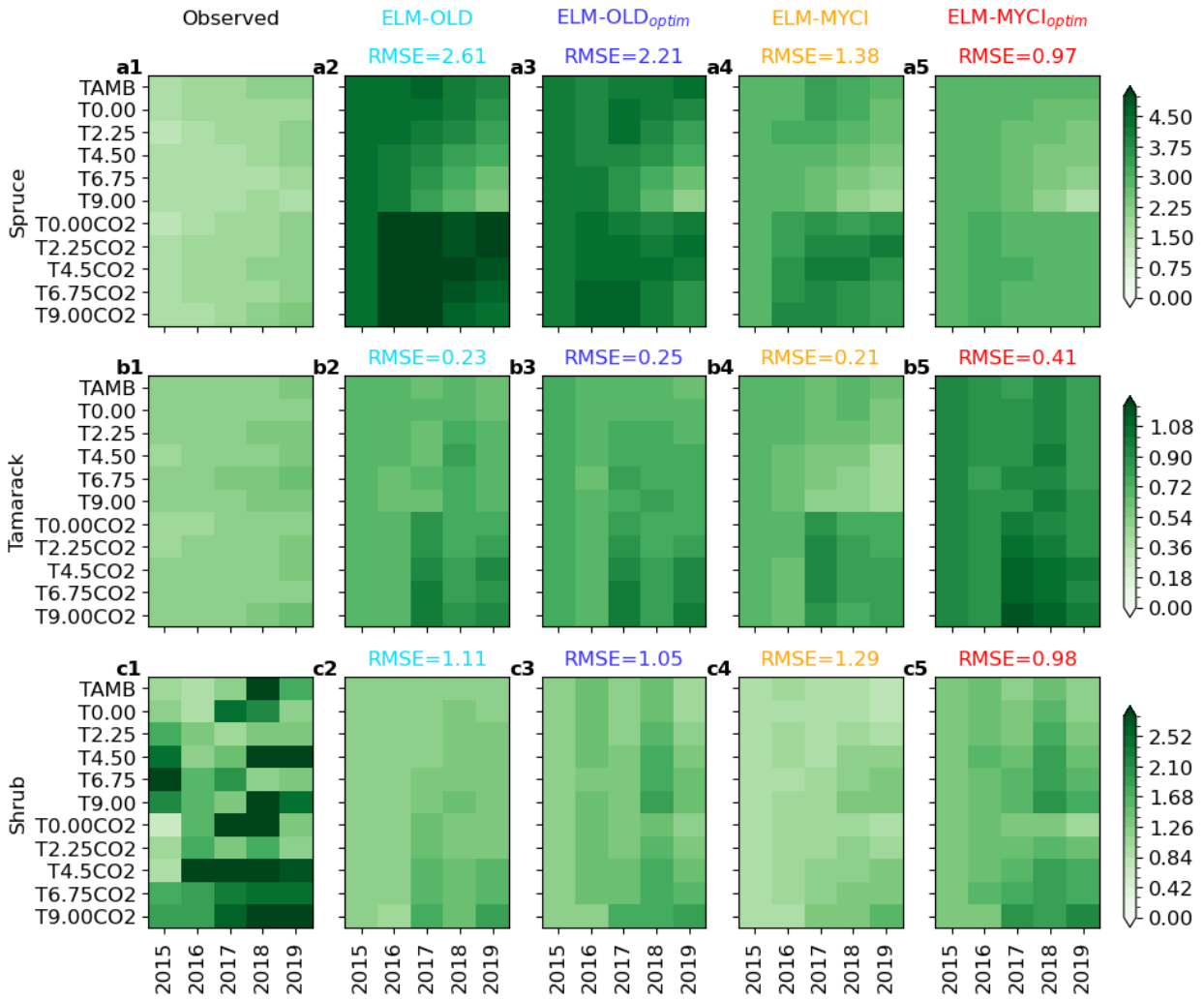

Figure S8. Observed annual maximum leaf area index and the corresponding simulated levels by the four model setups (m^2 m^{-2} ground area).

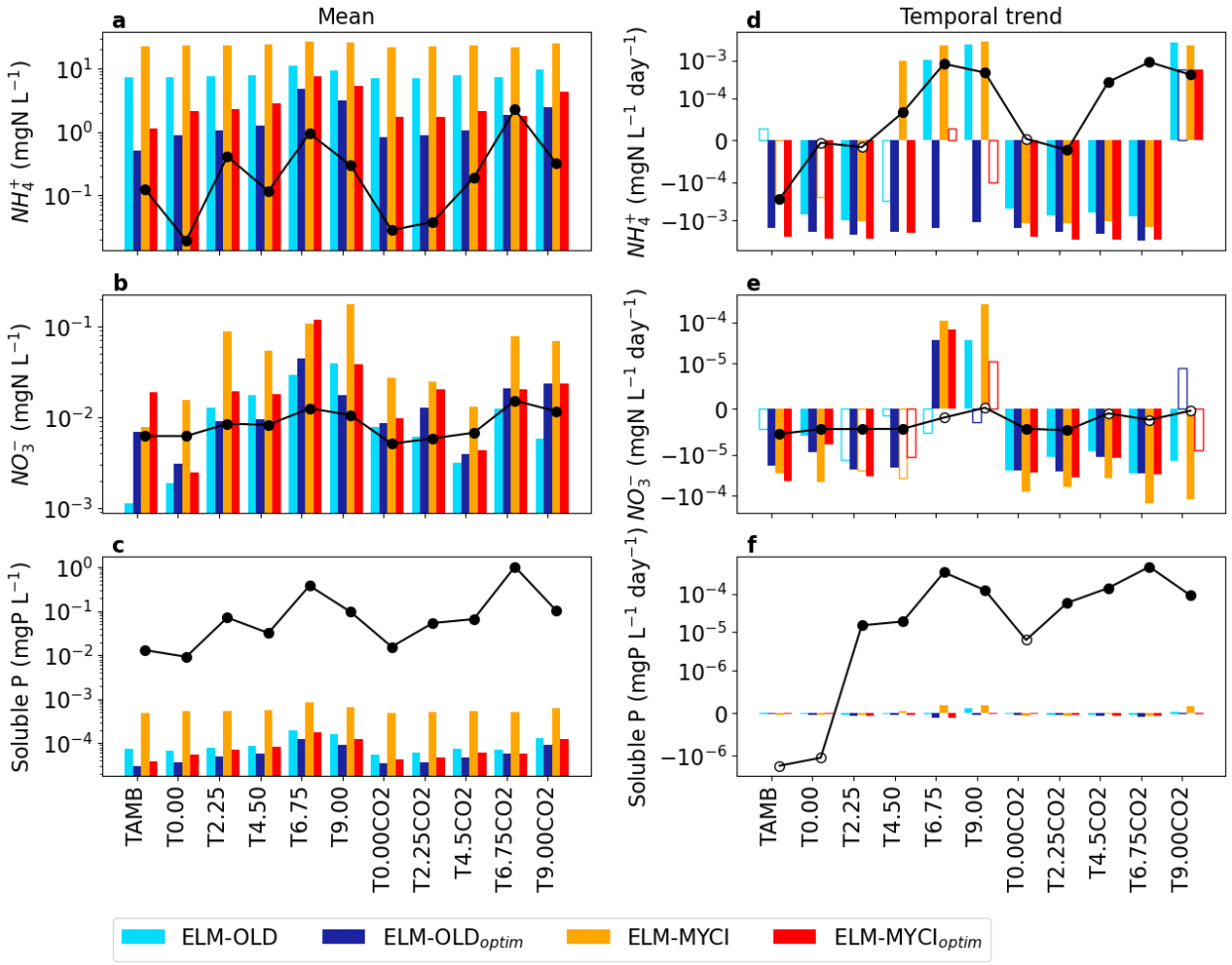

Figure S9. Observed and simulated mean values and least squares linear temporal trends in hollow soil pore water nutrient concentrations at 30cm depth during 2015-2020. Logscale is used because the modeled and observed values differ by orders of magnitudes. For the temporal trends, solid bars mean the trend is significant at p≤0.05 (two-sided t-test) and empty bars means insignificant.

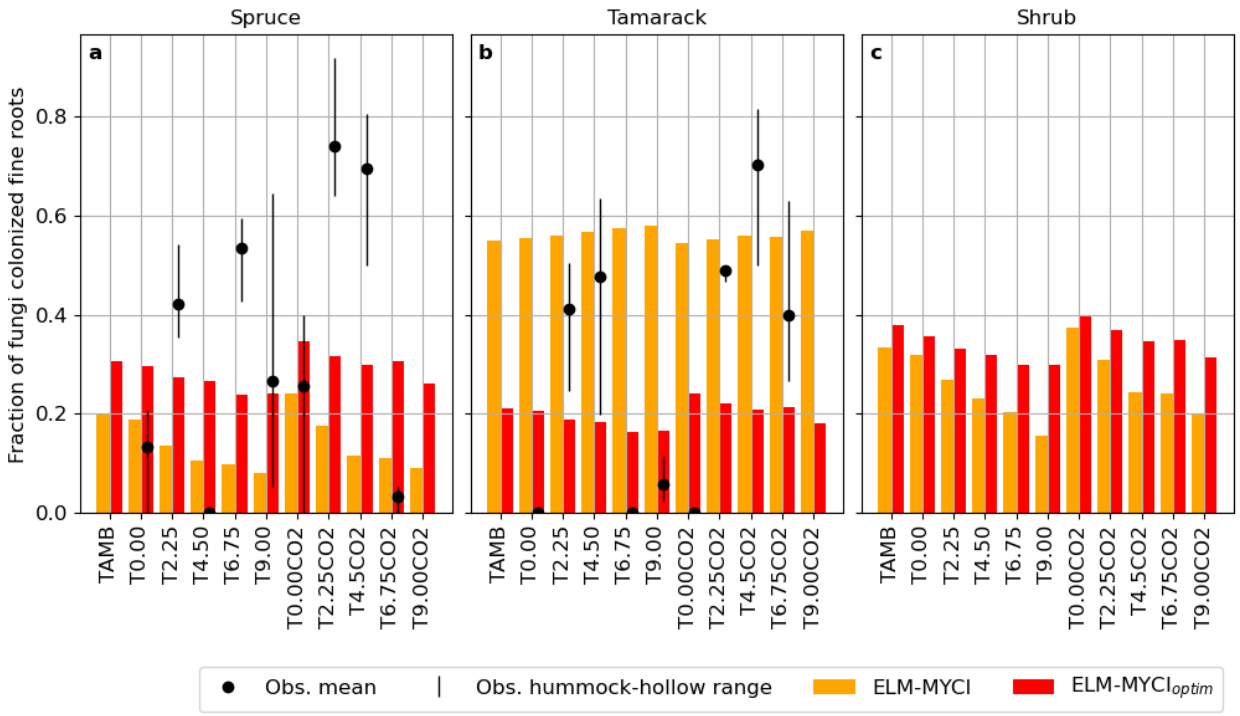

Figure S10. Fraction of fungi-colonized fine roots observed for tamarack in selected enclosures and simulated by the two modified model setups for spruce, tamarack, and shrub in all the enclosures. The observations were made in summer 2017, with one data point from the hummock and one from the hollow (Duchesneau et al., 2024). The display shows their weighted mean (0.64 × hummock + 0.36 × hollow) and the range. The simulated values are averaged over 2015-2021 for each enclosure and use the same hummock-hollow average (0.64 x hummock + 0.36 x hollow) as all the other modelled variables.

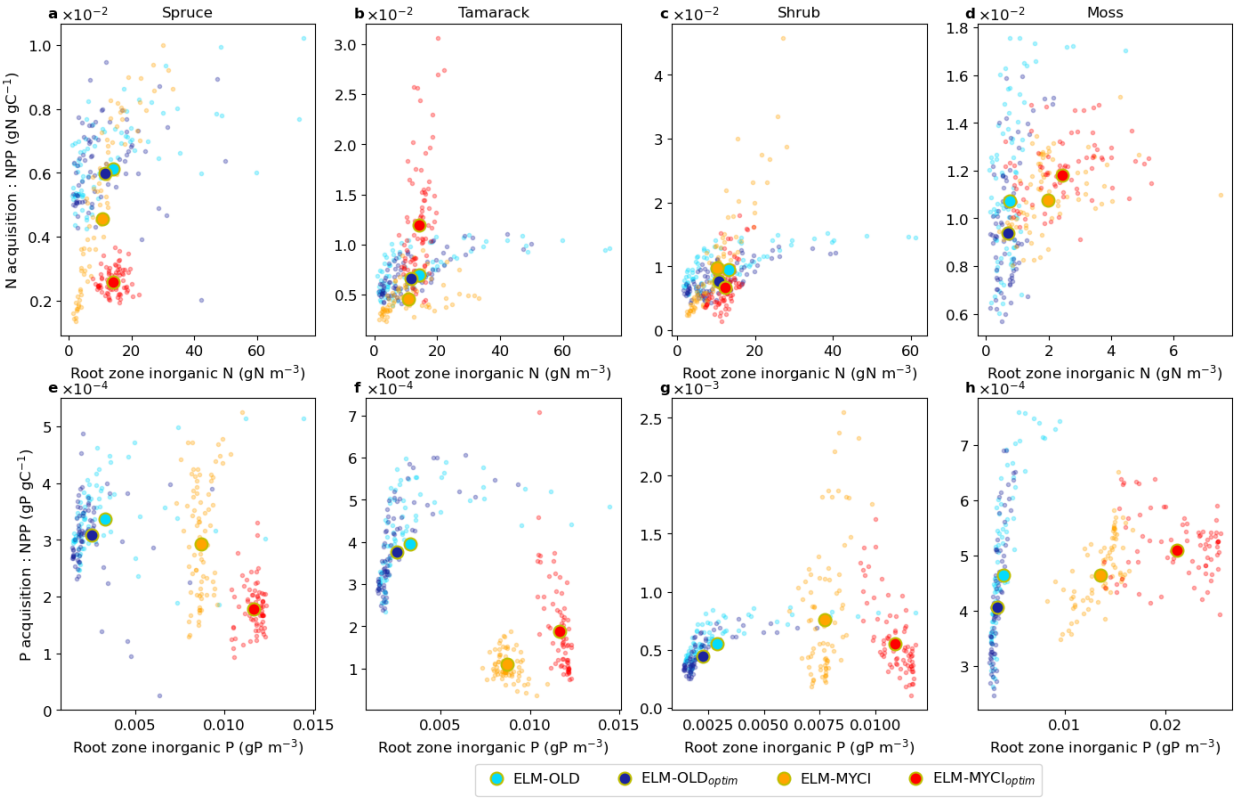

Figure S11. Relationship between the annual total NP acquisition per unit net primary productivity (NPP) and the annual mean soil inorganic nutrient content in different model setups. The total acquisition is equal to inorganic nutrient uptake in ELM-OLD and ELM-OLD$_{optim}$, and equal to the sum of all three pathways (actual inorganic nutrient uptake by uncolonized fine roots, actual inorganic nutrient uptake by mycorrhizal roots, and actual organic nutrient uptake by mycorrhizal roots) in ELM-MYCI and ELM-MYCI$_{optim}$. We normalize the acquisition to per unit NPP to remove the influences from vegetation biomasses and highlight the differences in the shapes of the relationships. Each small dot represents a single enclosure-year combination, and all the dots together span all the enclosures and 2015-2021. The large dots represent averages over all the years and chambers. The soil inorganic nutrient contents are weighted averages over all the soil layers using the plant functional type's fine-root fractions in each soil layer.

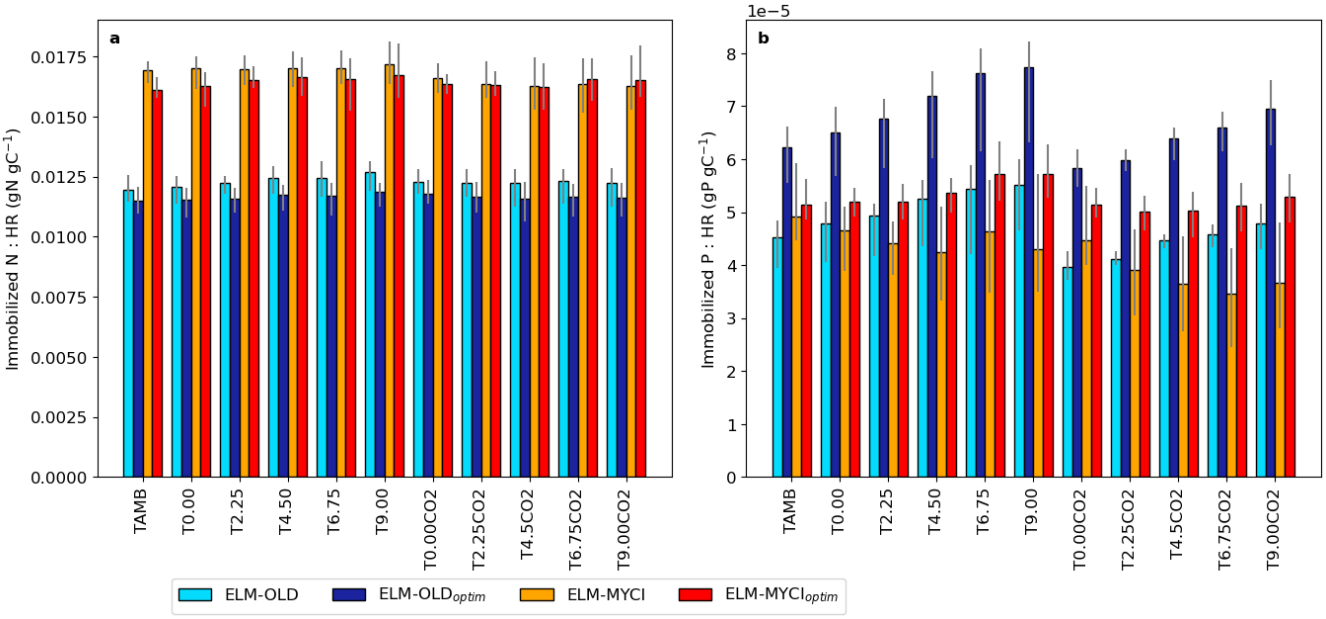

Figure S12. Ratio of annual mean actual immobilized NP to annual mean heterotrophic respiration (HR) in the soil decomposition process, across the enclosures. The bars show the mean values during 2015-2021 and errorbars show the ranges.

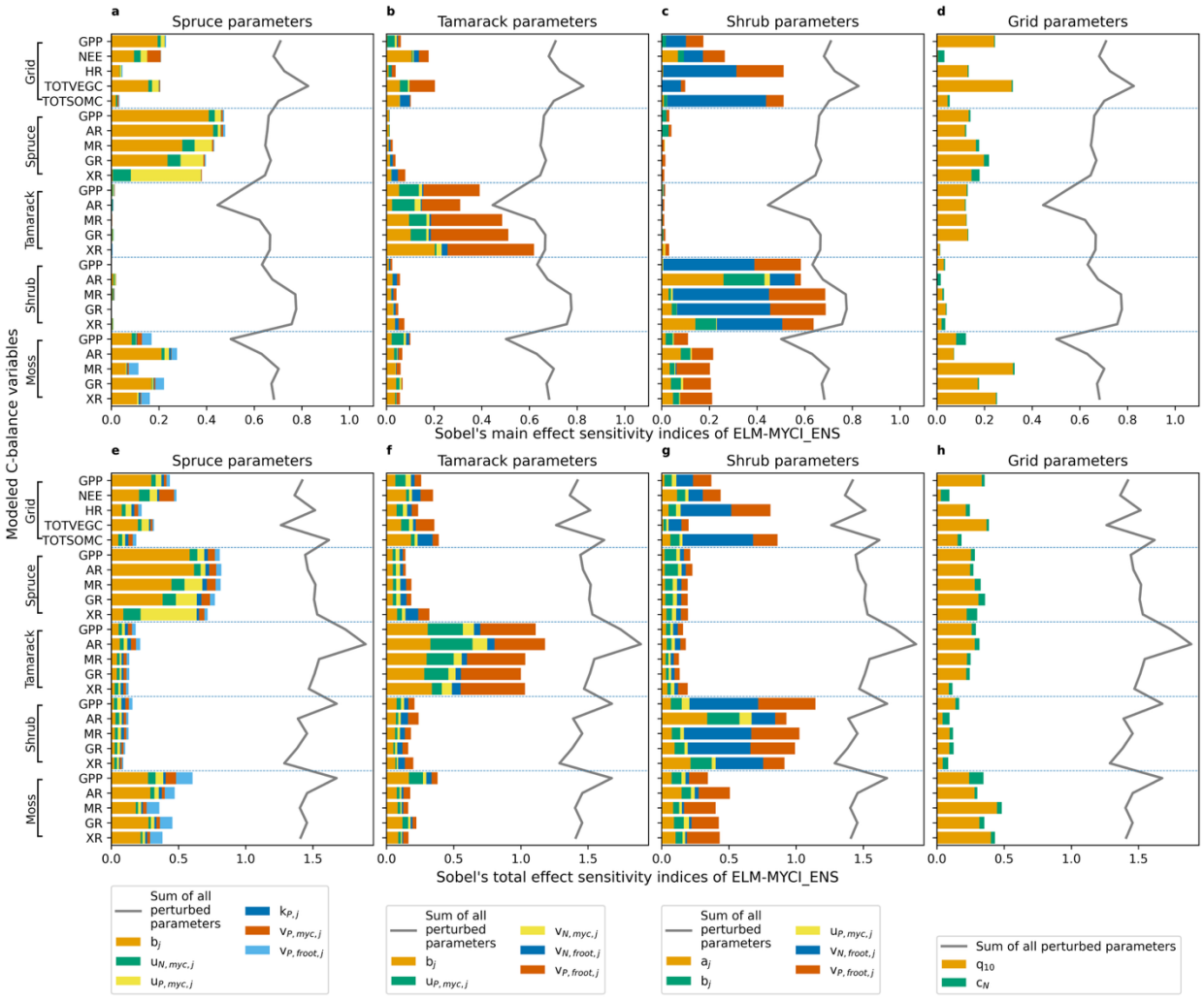

Figure S13. Sobol's main-effect and total-effect sensitivity indices of selected C-balance variables to the newly added model parameters, calculated from ELM-MYCI_ENS. For better display, the indices are partitioned into subpanels according to whether it is a PFT-specific or column-level parameter. Stacking the bars across the four panels in each row gives the sum of the main or total effects over all the perturbed parameters, which are also displayed as a grey line for reference in each panel. The C-balance variables in each panel are grouped according to whether it is a column-level, spruce, tamarack, shrub, or moss variable. Parameter definitions can be found in main text Table 1 and equations referred therein.

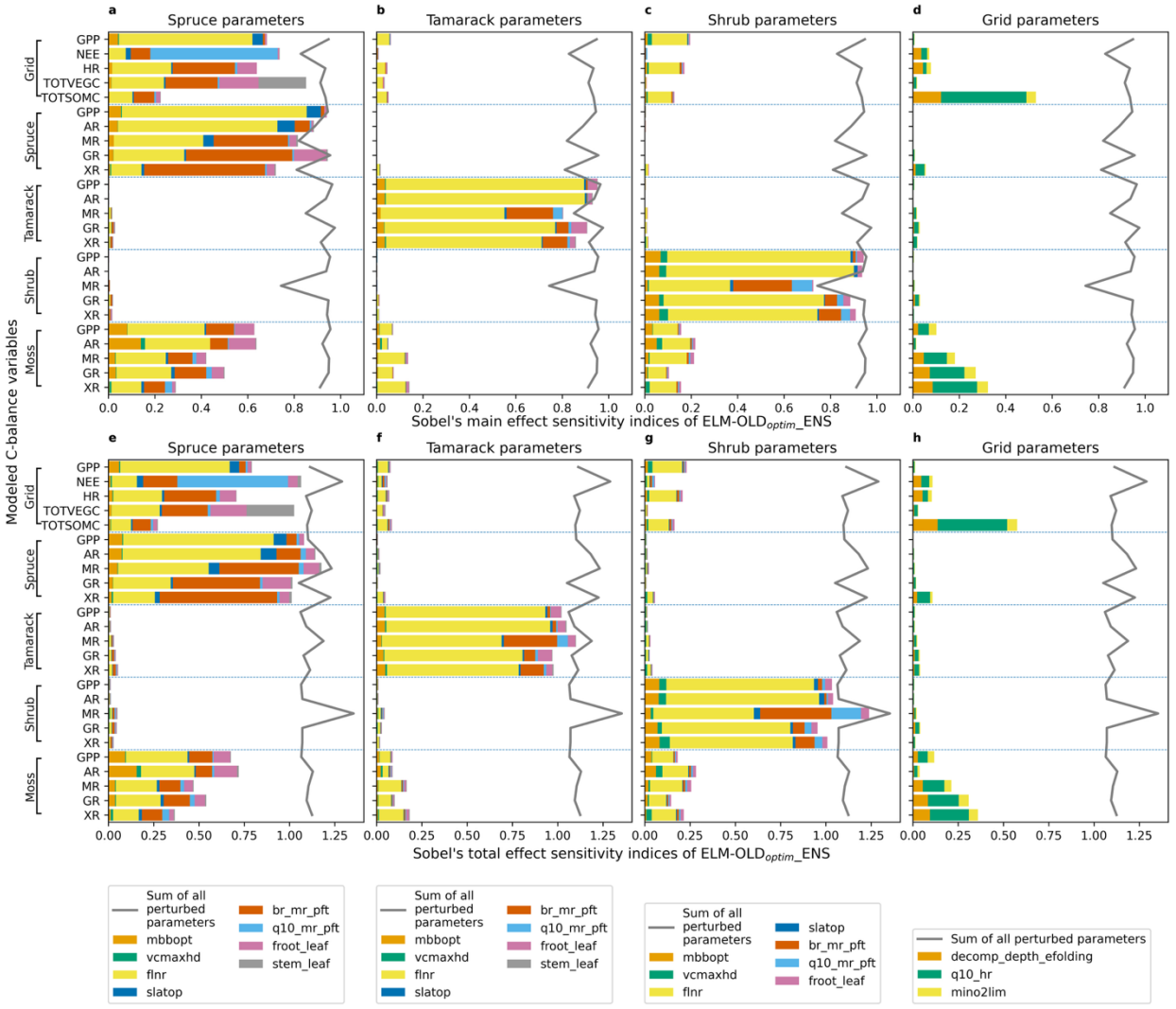

Figure S14. Sobol's main-effect and total-effect sensitivity indices of selected C-balance variables to the preexisting model parameters, calculated from ELM-OLD$_{optim}$_ENS. For better display, the indices are partitioned into subpanels according to whether it is a PFT-specific or column-level parameter. Stacking the bars across the four panels in each column gives the sum of the main or total effects over all the perturbed parameters, which are also displayed as a grey line for reference in each panel. The C-balance variables in each panel are grouped according to whether it is a column-level, spruce, tamarack, shrub, or moss variable. Parameter definitions can be found in Table S3.

S4 References

Arndal, M. F., Merrild, M. P., Michelsen, A., Schmidt, I. K., Mikkelsen, T. N., and Beier, C.: Net root growth and nutrient acquisition in response to predicted climate change in two contrasting heathland species, Plant Soil, 369, 615–629, https://doi.org/10.1007/s11104-013-1601-8, 2013.

Bashian-Victoroff, C., Yanai, R. D., Horton, T. R., and Lamit, L. J.: Nitrogen and phosphorus additions affect fruiting of ectomycorrhizal fungi in a temperate hardwood forest, Fungal Ecology, 73, 101388, https://doi.org/10.1016/j.funeco.2024.101388, 2025.

Bergmann, J., Weigelt, A., van der Plas, F., Laughlin, D. C., Kuyper, T. W., Guerrero-Ramirez, N., Valverde-Barrantes, O. J., Bruelheide, H., Freschet, G. T., Iversen, C. M., Kattge, J., McCormack, M. L., Meier, I. C., Rillig, M. C., Roumet, C., Semchenko, M., Sweeney, C. J., van Ruijven, J., York, L. M., and Mommer, L.: The fungal collaboration gradient dominates the root economics space in plants, Sci. Adv., 6, eaba3756, https://doi.org/10.1126/sciadv.aba3756, 2020.

Burrows, S. M., Maltrud, M., Yang, X., Zhu, Q., Jeffery, N., Shi, X., Ricciuto, D., Wang, S., Bisht, G., Tang, J., Wolfe, J., Harrop, B. E., Singh, B., Brent, L., Baldwin, S., Zhou, T., Cameron-Smith, P., Keen, N., Collier, N., Xu, M., Hunke, E. C., Elliott, S. M., Turner, A. K., Li, H., Wang, H., Golaz, J. -C., Bond-Lamberty, B., Hoffman, F. M., Riley, W. J., Thornton, P. E., Calvin, K., and Leung, L. R.: The DOE E3SM v1.1 biogeochemistry configuration: Description and simulated ecosystem-climate responses to historical changes in forcing, J. Adv. Model Earth Syst., 12, https://doi.org/10.1029/2019MS001766, 2020.

Chalk, P. and Smith, C.: On inorganic N uptake by vascular plants: Can 15N tracer techniques resolve the NH_4^+ versus NO_3^- "preference" conundrum?, European Journal of Soil Science, 72, 1762–1779, https://doi.org/10.1111/ejss.13069, 2021.

Chapin, F. S., Moilanen, L., and Kielland, K.: Preferential use of organic nitrogen for growth by a non-mycorrhizal arctic sedge, Nature, 361, 150–153, https://doi.org/10.1038/361150a0, 1993.

Clemmensen, K. E., Durling, M. B., Michelsen, A., Hallin, S., Finlay, R. D., and Lindahl, B. D.: A tipping point in carbon storage when forest expands into tundra is related to mycorrhizal recycling of nitrogen, Ecology Letters, 24, 1193–1204, https://doi.org/10.1111/ele.13735, 2021.

Colpaert, J. V., Tichelen, K. K. V., Assche, J. a. V., and Laere, A. V.: Short-term phosphorus uptake rates in mycorrhizal and non-mycorrhizal roots of intact Pinus sylvestris seedlings, The New Phytologist, 143, 589–597, https://doi.org/10.1046/j.1469-8137.1999.00471.x, 1999.

Daryanto, S., Wang, L., Gilhooly, W. P., III, and Jacinthe, P.-A.: Nitrogen preference across generations under changing ammonium nitrate ratios, Journal of Plant Ecology, 12, 235–244, https://doi.org/10.1093/jpe/rty014, 2019.

Defrenne, C. E., Childs, J., Fernandez, C. W., Taggart, M., Nettles, W. R., Allen, M. F., Hanson, P. J., and Iversen, C. M.: High-resolution minirhizotrons advance our understanding of root-fungal dynamics in an experimentally warmed peatland, Plants, People, Planet, 3, 640–652, https://doi.org/10.1002/ppp3.10172, 2021.

Duchesneau, K., Defrenne, C., Petro, C., Malhotra, A., Moore, J., Childs, J., Hanson, P., Iversen, C., and Kostka, J.: SPRUCE root tip and ectomycorrhizal fungi colonization measurements from ingrowth cores, 2017, https://doi.org/10.25581/SPRUCE.119/2476173, 2024.

Forsmark, B., Nordin, A., Rosenstock, N. P., Wallander, H., and Gundale, M. J.: Anthropogenic nitrogen enrichment increased the efficiency of belowground biomass production in a boreal forest, Soil Biology and Biochemistry, 155, 108154, https://doi.org/10.1016/j.soilbio.2021.108154, 2021.

Frolking, S., Roulet, N. T., Moore, T. R., Lafleur, P. M., Bubier, J. L., and Crill, P. M.: Modeling seasonal to annual carbon balance of Mer Bleue Bog, Ontario, Canada, Global Biogeochemical Cycles, 16, 4-1-4–21, https://doi.org/10.1029/2001GB001457, 2002.

Glass, A. D. M., Britto, D. T., Kaiser, B. N., Kinghorn, J. R., Kronzucker, H. J., Kumar, A., Okamoto, M., Rawat, S., Siddiqi, M. Y., Unkles, S. E., and Vidmar, J. J.: The regulation of nitrate and ammonium transport systems in plants, Journal of Experimental Botany, 53, 855–864, https://doi.org/10.1093/jexbot/53.370.855, 2002.

Glauch, T., Marshall, J., Gerbig, C., Botía, S., Gałkowski, M., Vardag, S. N., and Butz, A.: *pyVPRM*: a next-generation vegetation photosynthesis and respiration model for the post-MODIS era, Geoscientific Model Development, 18, 4713–4742, https://doi.org/10.5194/gmd-18-4713-2025, 2025.

Griffiths, N. A., Hanson, P. J., Ricciuto, D. M., Iversen, C. M., Jensen, A. M., Malhotra, A., McFarlane, K. J., Norby, R. J., Sargsyan, K., Sebestyen, S. D., Shi, X., Walker, A. P., Ward, E. J., Warren, J. M., and Weston, D. J.: Temporal and spatial variation in peatland carbon cycling and implications for interpreting responses of an ecosystem-scale warming experiment, Soil Science Society of America Journal, 81, 1668–1688, https://doi.org/10.2136/sssaj2016.12.0422, 2017.

Hanson, P. J., Riggs, J. S., Nettles, W. R., Krassovski, M. B., and Hook, L. A.: SPRUCE whole ecosystems warming (WEW) environmental data beginning august 2015, Oak Ridge National Laboratory, TES SFA, U.S. Department of Energy, Oak Ridge, Tennessee, U.S.A., https://doi.org/10.3334/CDIAC/spruce.032, 2016.

Hawkins, B. J., Boukcim, H., and Plassard, C.: A comparison of ammonium, nitrate and proton net fluxes along seedling roots of Douglas-fir and lodgepole pine grown and measured with different inorganic nitrogen sources, Plant, Cell & Environment, 31, 278–287, https://doi.org/10.1111/j.1365-3040.2007.01760.x, 2008.

Hawkins, H.-J., Cargill, R. I. M., Van Nuland, M. E., Hagen, S. C., Field, K. J., Sheldrake, M., Soudzilovskaia, N. A., and Kiers, E. T.: Mycorrhizal mycelium as a global carbon pool, Current Biology, 33, R560–R573, https://doi.org/10.1016/j.cub.2023.02.027, 2023.

He, H., Meyer, A., Jansson, P.-E., Svensson, M., Rütting, T., and Klemedtsson, L.: Simulating ectomycorrhiza in boreal forests: implementing ectomycorrhizal fungi model MYCOFON in CoupModel (v5), Geoscientific Model Development, 11, 725–751, https://doi.org/10.5194/gmd-11-725-2018, 2018.

He, H., Jansson, P.-E., and Gärdenäs, A. I.: CoupModel (v6.0): an ecosystem model for coupled phosphorus, nitrogen, and carbon dynamics – evaluated against empirical data from a climatic and fertility gradient in Sweden, Geoscientific Model Development, 14, 735–761, https://doi.org/10.5194/gmd-14-735-2021, 2021.

Hobbie, E. A. and Högberg, P.: Nitrogen isotopes link mycorrhizal fungi and plants to nitrogen dynamics, New Phytologist, 196, 367–382, https://doi.org/10.1111/j.1469-8137.2012.04300.x, 2012.

Högberg, M. N., Briones, M. J. I., Keel, S. G., Metcalfe, D. B., Campbell, C., Midwood, A. J., Thornton, B., Hurry, V., Linder, S., Näsholm, T., and Högberg, P.: Quantification of effects of season and nitrogen supply on tree below-ground carbon transfer to ectomycorrhizal fungi and other soil organisms in a boreal pine forest, New Phytologist, 187, 485–493, https://doi.org/10.1111/j.1469-8137.2010.03274.x, 2010.

Iversen, C. M., McCormack, M. L., Powell, A. S., Blackwood, C. B., Freschet, G. T., Kattge, J., Roumet, C., Stover, D. B., Soudzilovskaia, N. A., Valverde-Barrantes, O. J., Van Bodegom, P. M., and Violle, C.: A global Fine-Root Ecology Database to address below-ground challenges in plant ecology, New Phytologist, 215, 15–26, https://doi.org/10.1111/nph.14486, 2017.

Iversen, C. M., Childs, J., Norby, R. J., Ontl, T. A., Kolka, R. K., Brice, D. J., McFarlane, K. J., and Hanson, P. J.: Fine-root growth in a forested bog is seasonally dynamic, but shallowly distributed in nutrient-poor peat, Plant Soil, 424, 123–143, https://doi.org/10.1007/s11104-017-3231-z, 2018.

Iversen, C. M., Brice, D. J., Childs, J., Vander Stel, H. M., and Salmon, V. G.: SPRUCE S1 bog production of newly-grown fine roots assessed using root ingrowth cores in 2013, Oak Ridge National Laboratory, TES SFA, U.S. Department of Energy, Oak Ridge, Tennessee, U.S.A., https://doi.org/10.25581/spruce.091/1782483, 2021.

Kosola, K. R., Workmaster, B. A. A., and Spada, P. A.: Inoculation of cranberry (*Vaccinium macrocarpon*) with the ericoid mycorrhizal fungus *Rhizoscyphus ericae* increases nitrate influx, New Phytologist, 176, 184–196, https://doi.org/10.1111/j.1469-8137.2007.02149.x, 2007.

Lasslop, G., Reichstein, M., Papale, D., Richardson, A. D., Arneth, A., Barr, A., Stoy, P., and Wohlfahrt, G.: Separation of net ecosystem exchange into assimilation and respiration using a light response curve approach: critical issues and global evaluation, Global Change Biology, 16, 187–208, https://doi.org/10.1111/j.1365-2486.2009.02041.x, 2010.

Malhotra, A., Brice, D. J., Childs, J., Graham, J. D., Hobbie, E. A., Vander Stel, H., Feron, S. C., Hanson, P. J., and Iversen, C. M.: Peatland warming strongly increases fine-root growth, Proc. Natl. Acad. Sci. U.S.A., 117, 17627–17634, https://doi.org/10.1073/pnas.2003361117, 2020.

McCormack, M. L., Dickie, I. A., Eissenstat, D. M., Fahey, T. J., Fernandez, C. W., Guo, D., Helmisaari, H., Hobbie, E. A., Iversen, C. M., Jackson, R. B., Leppälammi-Kujansuu, J., Norby, R. J., Phillips, R. P., Pregitzer, K. S., Pritchard, S. G., Rewald, B., and Zadworny, M.: Redefining fine roots improves understanding of below-ground contributions to terrestrial biosphere processes, New Phytologist, 207, 505–518, https://doi.org/10.1111/nph.13363, 2015.

Meng, L., Mao, J., Ricciuto, D. M., Shi, X., Richardson, A. D., Hanson, P. J., Warren, J. M., Zhou, Y., Li, X., Zhang, L., and Schädel, C.: Evaluation and modification of ELM seasonal deciduous phenology against observations in a southern boreal peatland forest, Agric. For. Meteorol., 308–309, 108556, https://doi.org/10.1016/j.agrformet.2021.108556, 2021.

Norby, R. J., Childs, J., Hanson, P. J., and Warren, J. M.: Rapid loss of an ecosystem engineer: *Sphagnum* decline in an experimentally warmed bog, Ecology and Evolution, 9, 12571–12585, https://doi.org/10.1002/ece3.5722, 2019.

Oleson, K. W., Lawrence, D. M., Bonan, G. B., Drewniak, B., Huang, M., Levis, S., Li, F., Riley, W. J., Swenson, S. C., Thornton, P. E., Bozbiyik, A., Fisher, R., Heald, C. L., Kluzek, E., Lamarque, F., Lawrence, P. J., Leung, L. R., Muszala, S., Ricciuto, D. M., Sacks, W., Sun, Y., Tang, J., and Yang, Z.-L.: Technical Description of version 4.5 of the Community Land Model (CLM), National Center for Atmospheric Research, Boulder, CO, USA, 2013.

Phillips, J. R., Brice, D. J., Hanson, P. J., Childs, J., Iversen, C. M., Norby, R. J., and Warren, J. M.: SPRUCE pretreatment plant tissue analyses, 2009 through 2013, Oak Ridge National Laboratory, TES SFA, U.S. Department of Energy, Oak Ridge, Tennessee, U.S.A., https://doi.org/10.3334/CDIAC/spruce.038, 2017.

Renaudin, M., Khlifa, R., Legault, S., Kembel, S. W., Kneeshaw, D., Moore, J.-D., and Houle, D.: Long-term simulated nitrogen deposition has moderate impacts on soil microbial communities across three bioclimatic domains of the eastern Canadian forest, Forests, 14, 1124, https://doi.org/10.3390/f14061124, 2023.

Ricciuto, D., Sargsyan, K., and Thornton, P.: The impact of parametric uncertainties on biogeochemistry in the E3SM Land Model, J. Adv. Model. Earth Syst., 10, 297–319, https://doi.org/10.1002/2017MS000962, 2018.

Rossi, S., Bordeleau, A., Houle, D., and Morin, H.: Effect of chronic ammonium nitrate addition on the ectomycorrhizal community in a black spruce stand, Can. J. For. Res., 42, 1204–1212, https://doi.org/10.1139/x11-176, 2012.

Salmon, V. G., Brice, D. J., Bridgham, S., Childs, J., Graham, J., Griffiths, N. A., Hofmockel, K., Iversen, C. M., Jicha, T. M., Kolka, R. K., Kostka, J. E., Malhotra, A., Norby, R. J., Phillips, J. R., Ricciuto, D., Schadt, C. W., Sebestyen, S. D., Shi, X., Walker, A. P., Warren, J. M., Weston, D. J., Yang, X., and Hanson, P. J.: Nitrogen and phosphorus cycling in an ombrotrophic peatland: a benchmark for assessing change, Plant Soil, 466, 649–674, https://doi.org/10.1007/s11104-021-05065-x, 2021.

Sanders-DeMott, R., Sorensen, P. O., Reinmann, A. B., and Templer, P. H.: Growing season warming and winter freeze–thaw cycles reduce root nitrogen uptake capacity and increase soil solution nitrogen in a northern forest ecosystem, Biogeochemistry, 137, 337–349, https://doi.org/10.1007/s10533-018-0422-5, 2018.

Shao, S., Wu, J., He, H., Moore, T. R., Bubier, J., Larmola, T., Juutinen, S., and Roulet, N. T.: Ericoid mycorrhizal fungi mediate the response of ombrotrophic peatlands to fertilization: a modeling study, New Phytol., 238, 80–95, https://doi.org/10.1111/nph.18555, 2023.

Stelling, J. M., Mayes, M. A., Hanson, P. J., and Krassovski, M.: SPRUCE: Carbon dioxide and methane soil flux measurements at high temporal resolution, beginning in 2022, Oak Ridge National Laboratory, TES SFA, U.S. Department of Energy, Oak Ridge, Tennessee, USA, https://doi.org/10.25581/spruce.104/1922635, 2024.

Struyf, E., Kotowski, W., Jacobs, S., Van Damme, S., Bal, K., Opdekamp, W., Backx, H., Van Pelt, D., and Meire, P.: Tracing Si–N–P ecosystem-pathways: is relative uptake in riparian vegetation influenced by soil waterlogging, mowing management and species diversity?, Hydrobiologia, 674, 41–50, https://doi.org/10.1007/s10750-011-0737-x, 2011.

Thornton, P. E. and Rosenbloom, N. A.: Ecosystem model spin-up: Estimating steady state conditions in a coupled terrestrial carbon and nitrogen cycle model, Ecological Modelling, 189, 25–48, https://doi.org/10.1016/j.ecolmodel.2005.04.008, 2005.

Van Tichelen, K. K. and Colpaert, J. V.: Kinetics of phosphate absorption by mycorrhizal and non-mycorrhizal Scots pine seedlings, Physiologia Plantarum, 110, 96–103, https://doi.org/10.1034/j.1399-3054.2000.110113.x, 2000.

Vesala, R., Kiheri, H., Hobbie, E. A., Van Dijk, N., Dise, N., and Larmola, T.: Atmospheric nitrogen enrichment changes nutrient stoichiometry and reduces fungal N supply to peatland ericoid mycorrhizal shrubs, Science of The Total Environment, 794, 148737, https://doi.org/10.1016/j.scitotenv.2021.148737, 2021.

Walker, A. P., Carter, K. R., Gu, L., Hanson, P. J., Malhotra, A., Norby, R. J., Sebestyen, S. D., Wullschleger, S. D., and Weston, D. J.: Biophysical drivers of seasonal variability in *Sphagnum* gross primary production in a northern temperate bog, JGR Biogeosciences, 122, 1078–1097, https://doi.org/10.1002/2016JG003711, 2017.

Ward, E. B., Duguid, M. C., Kuebbing, S. E., Lendemer, J. C., and Bradford, M. A.: The functional role of ericoid mycorrhizal plants and fungi on carbon and nitrogen dynamics in forests, New Phytol., 235, 1701–1718, https://doi.org/10.1111/nph.18307, 2022.

Weber, S. E., Childs, J., Latimer, J., Hanson, P. J., Salmon, V. G., Schwaner, G., and Iversen, C. M.: Warming and elevated CO2 cause greater and deeper root growth by shrubs in a boreal bog, https://doi.org/10.1101/2025.06.26.661811, 30 June 2025.

Wu, Y. and Blodau, C.: PEATBOG: a biogeochemical model for analyzing coupled carbon and nitrogen dynamics in northern peatlands, Geosci. Model Dev., 6, 1173–1207, https://doi.org/10.5194/gmd-6-1173-2013, 2013.

Xie, L., Zhou, X., Liu, Q., Zhao, C., and Yin, C.: Inorganic nitrogen uptake rate of *Picea asperata* curtailed by fine root acclimation to water and nitrogen supply and further by ectomycorrhizae, Physiologia Plantarum, 173, 2130–2141, https://doi.org/10.1111/ppl.13562, 2021.